NATIONAL TECHNICAL UNIVERSITY OF ATHENS

POST GRADUATE PROGRAM IN COMPUTATIONAL MECHANICS

MULTISCALE MODELING OF GRAPHENE REINFORCED COMPOSITES

Master Thesis submitted

By

Panagiotis Seventekidis

Supervisor: Vissarion Papadopoulos, Assistant Professor N.T.U.A. School of Civil Engineering

February 2016

Athens

NATIONAL TECHNICAL UNIVERSITY OF ATHENS

POST GRADUATE PROGRAM IN COMPUTATIONAL MECHANICS

MULTISCALE MODELING OF GRAPHENE REINFORCED COMPOSITES

Master Thesis submitted

By

Panagiotis Seventekidis

Supervisor: Vissarion Papadopoulos, Assistant Professor N.T.U.A. School of Civil Engineering

February 2016

Athens

ΕΘΝΙΚΟ ΜΕΤΣΟΒΕΙΟ ΠΟΛΥΤΕΧΝΕΙΟ

ΔΙΑΤΜΗΜΑΤΙΚΟ ΠΡΟΓΡΑΜΜΑ ΜΕΤΑΠΤΥΧΙΑΚΩΝ ΣΠΟΥΔΩΝ ΣΤΗΝ ΥΠΟΛΟΓΙΣΤΙΚΗ ΜΗΧΑΝΙΚΗ

ΜΟΝΤΕΛΟΠΟΙΗΣΗ ΠΟΛΛΑΠΛΩΝ ΚΛΙΜΑΚΩΝ ΣΥΝΘΕΤΩΝ ΥΛΙΚΩΝ ΓΡΑΦΕΝΙΟΥ

Μεταπτυχιακή εργασία

του

Παναγιώτη Σεβεντεκίδη

Επιβλέπων:Βησσαρίων Παπαδόπουλος, Επίκουρος Καθηγητής Ε.Μ.Π. Σχολή Πολιτικών Μηχανικών

Φεβρουάριος 2016

Αθήνα

Ευχαριστίες

Η παρούσα μεταπτυχιακή εργασία σηματοδοτεί το τέλος των σπουδών μου στο Διατμηματικό Πρόγραμμα Μετατπυχιακών Σπουδών στην Υπολογιστική Μηχανική. Στο σημείο αυτό θα ήθελα να ευχαριστήσω ιδιαίτερα τον Επίκουρο Καθηγητή της Σχολής Πολιτικών Μηχανικών, κύριο Βησσαρίων Παπαδόπουλο, που μου παρείχε την ευκαιρία εκπόνησης της παρούσας εργασίας. Η βοήθειά και υποστήριξή του στην ανάπτυξη της εργασίας κρίθηκε σημαντική, διευρύνοντας τις γνώσεις μου στα θέματα μηχανικής των νανοσύνθετων υλικών. Θερμές ευχαριστίες οφείλω επίσης στην οικογένειά μου για την εμπιστοσύνη και υποστήριξη που μου έχουν δείξει.

Contents

Περίληψη

Στην παρούσα μεταπτυχιακή εργασία, αναλύεται η ανάπτυξη του ισοδύναμου συνεχούς μέσου μοντέλου του γραφενίου σε πολλαπλές κλίμακες, χρησιμοποιώντας πεπερασμένα στοιχεία κελύφους. Το ισοδύναμο μοντέλο χρησιμοποιείται στη συνέχεια για την ανάλυση και προσομοίωση νανοσύνθετων πολυμερών υλικών, λαμβάνοντας υπόψη την επίδραση της διεπιφανειακής αντοχής στις μηχανικές ιδιότητες. Οι προσομοιώσεις που παρουσιάζονται, βασίζονται στη χρήση κλασσικών πεπερασμένων στοιχείων συνεχούς μέσου για τη μοντελοποίηση των ατομικών αλληλεπιδράσεων στο πλέγμα άνθρακα του γραφενίου. Σύμφωνα με θεωρήσεις δομικής μοριακής μηχανικής, το πεδίο δυνάμεων που ορίζει τις αλληλεπιδράσεις μεταξύ των ατόμων, μπορεί να αντικατασταθεί από κλασσικά πεπερασμένα στοιχεία δοκού. Οι μηχανικές και γεωμετρικές ιδιότητες αυτών μπορούν να υπολογιστούν αναλυτικά. Παρέχεται έτσι μεγάλη ακρίβεια στις μηχανικές ιδιότητες του προσομοιώματος. Για την επίτευξη ενός υπολογιστικά χαμηλού κόστους μοντέλου, το πλέγμα των πεπερασμένων στοιχείων δοκού αντικαθιστάται από κλασσικά πεπερασμένα στοιχεία κελύφους. Ο υπολογισμός των μηχανικών σταθερών και του πάχους αυτών, γίνεται με αλγόριθμο βελτιστοποίησης, κάνοντας χρήση κριτηρίων ισοδύναμης ενέργειας παραμόρφωσης και μετατοπίσεων σε σύγκριση με το αρχικό προσομοίωμα δοκών. Σαν αποτέλεσμα έχουμε υψηλή ακρίβεια σε πολλαπλές κλίμακες και πολύ χαμηλότερο υπολογιστικό κόστος σε σχέση με το αρχικό μοντέλο στοιχείων δοκού. Το ισοδύναμο συνεχές που αποτελείται πλεον από πεπερασμένα στοιχεία κελύφους, χρησιμοποιείται στη συνέχεια για την μοντελοποίηση νανοσύνθετου υλικού πολυμερικής μήτρας ενισχυμένο με γραφένιο. Για το νανοσύνθετο επιλέγεται αντιπροσωπευτικό στοιχείου όγκου, όπου το γραφένιο είναι ενσωματωμένο σε ορθωνική μήτρα πολυμερούς. Για τη μοντελοποίηση της μήτρας χρησιμοποιούνται τριδιάστατα πεπερασμένα στοιχεία 8 κόμβων και γραμμικές ελαστικές ιδιότητες υλικού. Ο μηχανισμός μεταφοράς δυνάμεων από την πολυμερική μήτρα στο γραφένιο επιτυγχάνεται μέσω της διεπιφάνειας αυτών, για την οποία ορίζεται επιφανειακή συμπεριφορά συνοχής (cohesive zone). Η συμπεριφορά αυτή έχει αποδειχθεί κατάλληλη για την ανάλυση της αστοχίας και ολίσθησης σύνθετων υλικών στη διεπιφάνεια. Το διάνυσμα τάσης μεταξύ των δύο επιφανειών, υπολογίζεται βάσει ενός καταστατικού νόμου ως συνάρτηση της απομάκρυνσης (traction-separation law), έχοντας επίσης τη δυνατότητα να ακολουθήσει προεπιλεγμένο μοντέλο αστοχίας. Με τον συγκεκριμένο τρόπο μοντελοποίησης είναι δυνατόν να μελετηθεί πως επιδρά στις μηχανικές ιδιότητες του νανοσύνθετου υλικού η τιμή της διεπιφανειακής αντοχής, καθώς και ο τρόπος αποκόλλησης για απλές ή ανακυκλιζόμενες φορτίσεις. Επίσης εξετάζονται γεωμετρικές ατέλειες, όπώς κυματισμοί στο γραφένιο. Τα αριθμητικά αποτελέσματα καταδεικνύουν ότι ο τρόπος μοντελοποίησης του γραφενίου με ισοδύναμα πεπερασμένα στοιχεία, είναι αποτελεσματικός για τη μοντελοποίηση σύνθετων υλικών σε πολλαπλές κλίμακες. Η επίδραση της διεπιφανειακής αντοχής και τα φαινόμενα ολίσθησης που προκύπτουν, κρίνονται σημαντικά στη μηχανική συμπεριφορά του υλικού, σε

συμφωνία επίσης με την αντίστοιχη βιβλιογραφία. Για τη γένεση πλεγμάτων και τους αλγορίθμους βελτιστοποίησης χρησιμοποιήθηκε το εμπορικό μαθηματικό πακέτο MATLAB. Για τις προσομοιώσεις πεπερασμένων στοιχείων στο γραφένιο και στο νανοσύνθετο υλικό, χρησιμοποιήθηκε το εμπορικό πακέτο ABAQUS.

Abstract

In the present work, a method is introduced for the development of the equivalent continuum model of graphene sheets, with shell finite elements in multiple scales. The equivalent continuum model is then used for the modeling of graphene nanocomposite materials, with respect to the effect of the interfacial strength on the mechanical behavior. The simulations presented, are based on the use of classic continuum finite elements for the representation of the interatomic interactions, in the hexagonal carbon lattice of graphene. According to Molecular Structural Mechanics, the force field that defines the interatomic interactions can be replaced with beam finite elements. The mechanical and geometrical properties of the beam elements are analytically calculated by making use of equivalent strain energy criteria, providing great accuracy in the mechanical properties of the model. For the reduction of the computational effort required in larger models, the beam element mesh is replaced with fewer shell elements, capturing the effects occurring in the multiple size scales. For the calculation of the mechanical and geometrical properties of the equivalent shell elements, an optimization algorithm is developed, searching for the solution with respect to strain energy and displacement criteria of the original beam element model. As a result, a high accuracy and much more computationally efficient model of graphene in multiple scales is derived. The equivalent shell model is then used as the filler in the polymer matrix of the nanocomposite. For the nanocomposite a representative volume element is chosen, where the graphene sheet is embedded in a rectangular matrix. For the modeling of the matrix three dimensional 8-nodded continuum finite elements with linear material properties are chosen. The load transferring mechanism between the matrix and the filler is modeled as a cohesive zone, which is suitable for the study of failure and occurring slippage along the interface. The cohesive behavior is defined with a traction-separation law, where the traction vector between the two surfaces is calculated as a function of the separation. A predefined damage propagation model based on plastic displacement criteria is followed. With this specific way of modeling, it is possible to study efficiently the effects of the interfacial strength on the mechanical properties and behavior of the nanocomposite, in simple or cyclic loading conditions. The numerical results presented, reveal that the equivalent shell element model of graphene is an effective modeling technique along multiple scales and can capture efficiently phenomena that occur in interfacial strength depended behavior. In addition, the effect of wrinkles on graphene is also highlighted in the present study. The results present good agreement with the currently available literature on composite and nanocomposite materials interfacial debonding and delamination studies. For the mesh generation and optimization algorithms the commercial mathematical package MATLAB was used. For the finite element simulations of the graphene sheets and graphene nanocomposites the commercial simulation package ABAQUS was used.

1 Introduction

Graphene as a new emerging material has attracted tremendous scientific interest, due to its extraordinary mechanical and electrical properties. An allotrope of carbon, graphene forms a hexagonal honeycomb lattice which can be one atom thick, known as single layer graphene sheet (SLGS) synthesized via various methods [1-3]. Graphene has been found to be the strongest material ever tested [4,5] with a Young's Modulus of 1 TPa and Tensile Strength of 130 GPa, making it a very promising material for structural applications. Graphene sheets (GS) and its derivative products the carbon nanontubes (CNT), have been successfully used as filler materials in nanostructured composites [6,7], greatly enchanching the mechanical properties of the matrix. Successful applications include both metal matrix [8,9] and polymer matrix [10,11] nanocomposites. The present work, aims to provide an efective way for the modeling of the mechanical behavior and properties of graphene nanocomposites in multiple scales. Two distinct points in the modeling process of graphene nanocomposites are presented in detail, first the method of simulation of graphene and second the load transferring mechanism between the matrix and the filler.

The modeling methods currently available for simulation of the mechanical behavior of graphene, take into account the interatomic interactions between the carbon atoms in the hexagonal lattice. Computational methods widely used, can be generally classified into two categories. One is the atomistic modeling [12,13] with major techniques including molecular mechanics and ab-initio calculations. The other way is the approach by continuum mechanics [14-16] including the analysis with finite element methods. Each of the above methods, comes with different performance along multiple time and size scales. Ab-initio and molecular mechanics techniques generally provide high accuracy at the smallest scales, but due to the high computational effort required, they are suitable for small size models and short time spans [16,17]. On the other hand, continuum mechanics techniques aim to provide accurate and computationally efficient models at larger size and time scales [17]. The accuracy of the continuum mechanics techniques depends greatly on the physical parameters of the equivalent continuum models, which replace the hexagonal lattice. Different continuum models with finite elements have been proposed [17-20].

The main principle behind continuum mechanics techniques, knows as Molecular Structural Mechanics (MSM), is the simulation of the covalent bonds between the carbon atoms, with equivalent structural finite elements [17]. The physical properties of the equivalent finite elements can be analytically calculated by making use of equivalent strain energy criteria, with reference to the force field that defines the interatomic interactions. Currently, the dominant method is replacing the carbon covalent bonds with beam finite elements, which can capture both stretching and rotation between atoms. While this approach is computationally effective

and accurate compared to the atomistic simulations [17-20], the computational effort increases dramatically while shifting time and size scales. For this reason the beam finite element model is replaced with an equivalent finite element mesh, aiming to provide a model with fewer finite elements but with the same degree of accuracy. The type of the elements to replace the beam frame depends on the initial geometry of model. This way of modeling has successfully found application in the simulation of the mechanical behavior of CNTs, where the beam element frame that represents the CNT, is replaced with an equivalent beam continuum element [21-23]. A lower element to volume ratio is then achieved, lowering the computational effort required and enabling more time or size demanding results to be achieved. The present work aims to develop an equivalent continuum model in multiple scales, which can replace the beam element frame of GSs rather than CNTs. GSs are found to have shell like behavior in relatively large models, compared to the beam like behavior of CNTs. The problem of finding an equivalent shell element (ESE) of a frame structure, while retaining the original size, is the calculation of the physical properties of the shells, being the Young's Modulus, Poisson's ratio and the equivalent thickness. The ESE should be able to accurately represent both the membrane and the plate behavior of the GS, and is thoroughly discussed in the following chapters.

The ESE of graphene is then embedded into a polymer matrix, for the study of the mechanical behavior of the nanocomposite. A representative volume element is chosen for the simulations. The load transferring mechanism between the matrix and the filler has been found to play a crucial role in the mechanical properties of nanocomposites. Numerical simulations indicate that the interfacial stiffness and strength, define the limits of mechanical enhancement of the nanocomposite by the filler and the occurring slippage when failure arises [21,24]. Techniques have been proposed for enchanced cohesion between the matrix and the filler [25,26]. A Load transferring mechanism via a friction model has been previously applied with success in modeling CNT nanocomposites [21,27]. In the present study, the interfacial load transferring mechanism is being modeled with a definition of cohesive behavior between the ESE and the three dimensional matrix. The cohesive behavior defines a traction-separation law between surfaces and can follow a predefined damage model. Cohesive elements have already been used to capture delamination and debonding phenomena for composite or nanocomposite materials [28-30] and reinforced steel [31], with good agreement with the experimental data.

The present work concludes with numerical results of the finite element simulations of graphene nanocomposites. The representation of the hexagonal carbon lattice with an ESE and the load transferring mechanism with a cohesive behavior, are found to be effective modeling techniques. The process followed can be summarized in Figure 1.

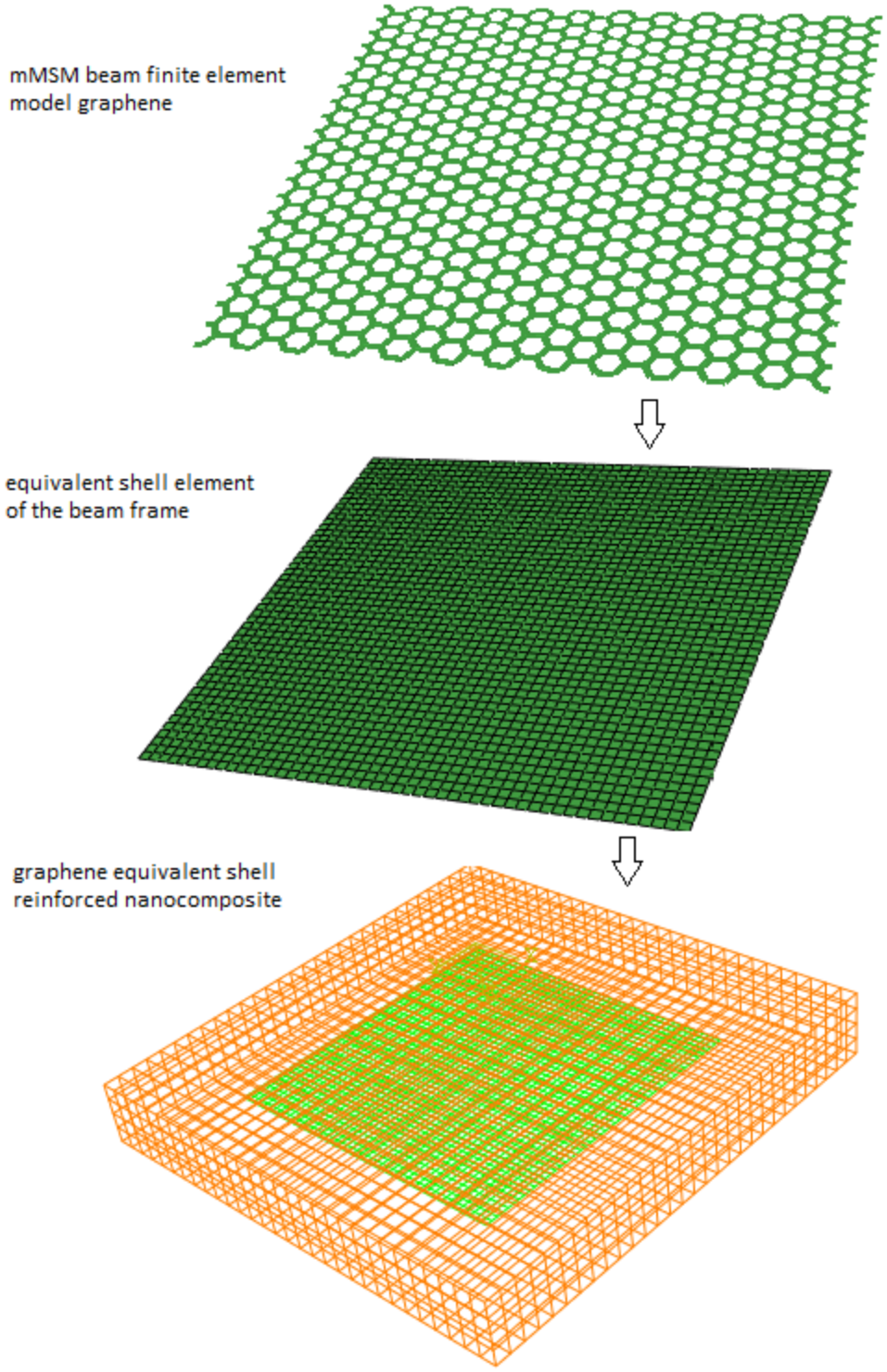

Figure 1: Summary of the process followed in the present work

2 The Finite Element Model of Graphene

2.1 The Molecular Structural Mechanics Approach

Molecular Structural Mechanics (MSM) finite element models have been found to be effective ways for the modeling of graphene and carbon nanotubes (CNTs). The MSM method, originally developed by Li and Chou [17], aims to provide a linkage between microscopic computational chemistry and macroscopic structural mechanics. Graphene sheets (GS) can be regarded as large molecules consisting of carbon atoms in a hexagonal honeycomb lattice. From the molecular mechanics point of view, atomic nuclei have their motions regulated by electron-nucleus and nucleus-nucleus interactions [32]. A representation of a GS hexagonal lattice can be shown in Figure 2.

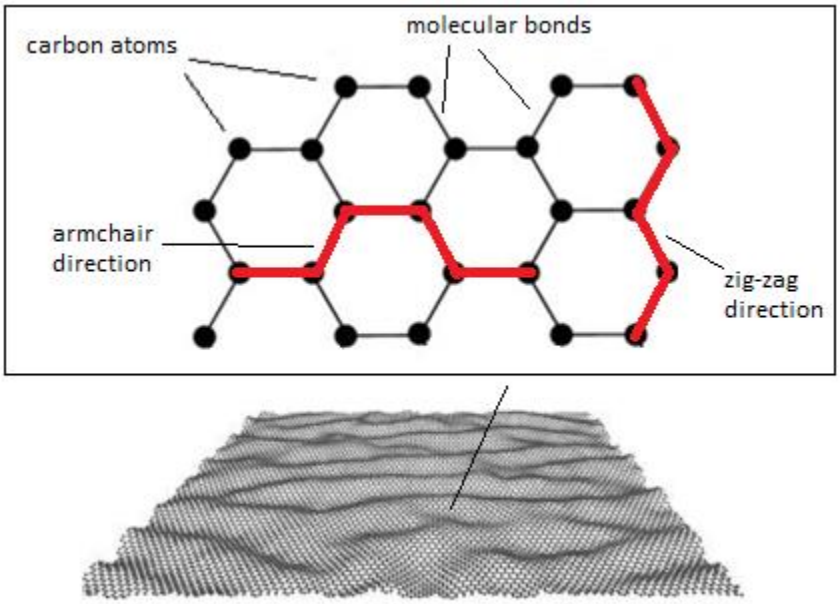

Figure 2: Representation of a GS hexagonal lattice

The force field that defines the interatomic interactions depends only on the relative positions of the nuclei, and can be expressed in the form of steric potential energy as:

$$U = \sum Ur + \sum U\theta + \sum U\phi + \sum U\omega + \sum Uvdw \qquad (1)$$

Where Ur is for bond stretching, Uθ for bond angle bending, Uϕ for dihedral angle torsion, Uω for out of plane torsion and Uvdw for Van der Waals interactions. The interactions and relative motions of the carbon atoms that correspond to the above relation are shown in Figure 3. In the present work, for simplicity and due to the assumptions of small deformations, harmonic approximation of the energy is adequate [17]. Considering Van der Waals interactions to be

negligible and merging the dihedral angle and improper torsion the energy components become:

$$Ur = \frac{1}{2}k\sigma(r - r0)^2 = \frac{1}{2}k\sigma\left(\Delta r\right)^2 \qquad (2)$$

$$U\theta = \frac{1}{2}k\theta\left(\theta - \theta 0\right)^2 = \frac{1}{2}k\theta\left(\Delta\theta\right)^2 \qquad (3)$$

$$U\tau = U\phi + U\omega = \frac{1}{2}k\tau\left(\Delta\phi\right)^2 \qquad (4)$$

Where kr, kθ, kτ are force field constants that correspond to Δr, Δθ and Δϕ relative motions. The force field constants can be selected from a suitable potential for graphene such as the AMBER [33] potential, where kr=938kcal×mole^{-1}×Å^{-2}=6.52×10^{-7} N/nm, kθ=126 kcal×mole^{-1}×rad^{-2}=8.76×10^{-10} Nnm rad^{-2} και kτ=40 kcal×mole^{-1}×rad-2=2.78×10^{-10}Nnm rad^{-2}.

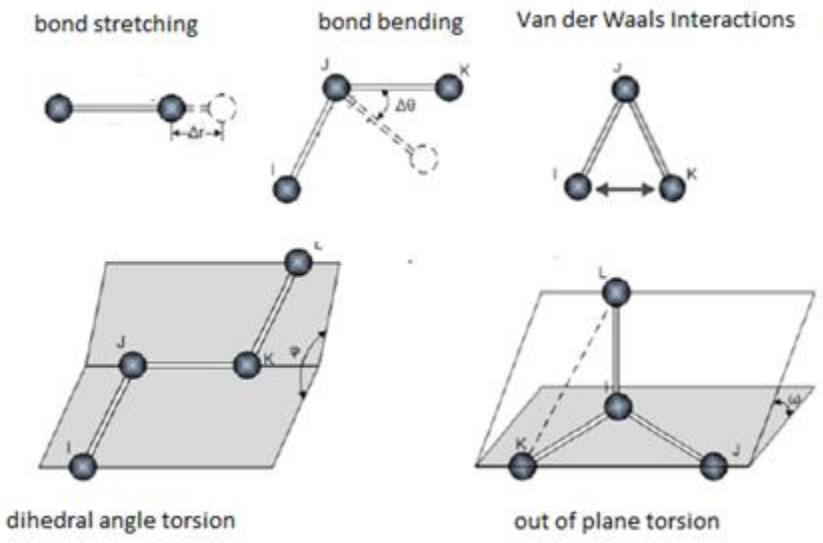

Figure 3: Interatomic interactions in the molecular mechanics of graphene

Further into the MSM approach, the similarity of the expressions between the molecular potential energy and the strain energy of a beam element is examined. For a uniform beam subjected to pure tension or compression of axial force N, the strain energy according to structural mechanics is:

$$UAx = \frac{1}{2}\int_0^L \frac{N^2}{EA}\,dL = \frac{1}{2}\frac{N^2L}{EA} = \frac{1}{2}\frac{EA}{L}\left(\Delta L\right)^2 \qquad (5)$$

The strain energy for pure bending under bending moment M is:

$$Ub = \frac{1}{2}\int_0^L \frac{M^2}{EI}\,dL = \frac{2EI}{L}\alpha^2 = \frac{1}{2}\frac{EI}{L}(2\alpha)^2 \qquad (6)$$

The strain energy for pure torsion under moment T is:

$$UT = \frac{1}{2}\int_0^L \frac{T^2}{GJ}\,dL = \frac{1}{2}\frac{T^2 L}{GJ} = \frac{1}{2}\frac{GJ}{L}(\Delta\beta)^2 \qquad (7)$$

In the above relations, ΔL in (5) represents the axial deformation, α in (6) the angle of rotation at the beam ends and Δβ the relative rotation between the beam ends. The loading conditions and deformations of the beam are depicted in Figure 4.

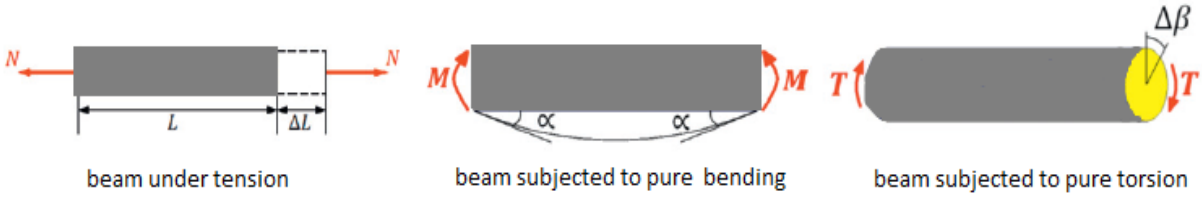

Figure 4: The loading conditions of the beam corresponding to equations 5-7

Comparing the equations (2-4) with the equations (5-7), the similarities in the energy terms and deformations are obvious. Both equation (2) and (5) represent stretching energy, equations (3) and (6) bending energy, and equations (4) and (7) torsional energy. Thus, the carbon-carbon bond can be simulated with a beam element with the following structural characteristics:

$$\frac{EA}{L} = k_r \qquad \frac{EI}{L} = k_\theta \qquad \frac{GJ}{L} = k_\tau \qquad (8)$$

In the MSM approach, the beam element constants E and G are derived in the simplest way as functions of the force field constants, assuming a beam of circular cross-section with diameter d, for which the parameters A, I and J are known as:

$$A = \frac{\pi d^2}{4} \qquad I = \frac{\pi d^4}{32} \qquad J = \frac{\pi d^4}{64} \qquad (10)$$

Substituting the relations in (10) to the relations in (8) the beam characteristics are derived as:

$$d = 4\sqrt{\frac{k\theta}{k\tau}} \qquad E = \frac{k\sigma^2 L}{4\pi k\theta} \qquad G = \frac{k\sigma^2 k\tau L}{8\pi k\theta^2} \qquad (11)$$

The length L of the beam is chosen to be L=0.1421nm which is the length of the covalent bond and the constants in (11) are be calculated as *d*=0.147 nm, *E*=5488 GPa, *G*=870.7 GPa. At this stage the MSM model is ready to be applied for the simulation of the mechanical behavior of a GS with beam finite elements. A beam finite elemet mesh, depicted in Figure 5, can be developed in a commercial simulation software package like ABAQUS. However, in the present work the beam finite element used, is based on a modified version of the MSM, suggesting that the MSM approach is suitable for in-plane loads only, due to the circular beam assumption.

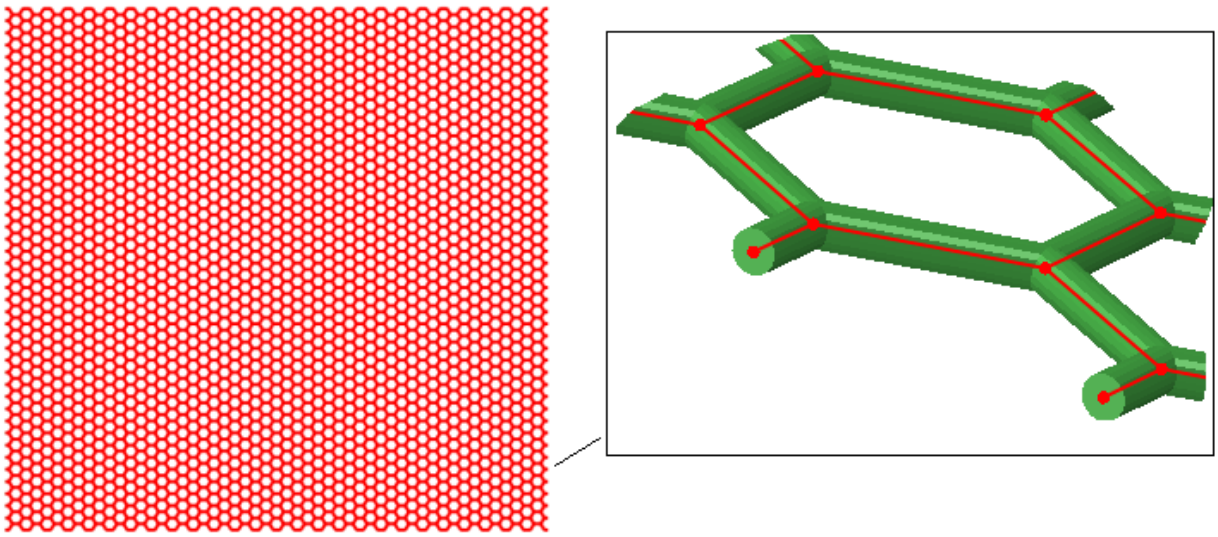

Figure 5: 11.08x10.58 nm circular beam finite element model of a GS

2.2 The Modified Molecular Mechanics Model

The Modified Molecular Structural Mechanics (mMSM) is a more accurate version of the MSM approach. In the MSM finite element model of graphene, circular cross-section for the beam elements was assumed, implying that the in-plane and out-of plane bending rigidities of the beam are equal. As stated by Lu and Hu [19] who proposed an elliptical cross-section for the beam, out of plane bending rigidity is largely overestimated in the MSM approach; fact supported both by atomistic and other analysis. Therefore, a suitable modified version of the MSM has to be taken into consideration. In the present work the finite element model for the GS, is based on a rectangular beam cross-section proposed by Chen [34]. According to the mMSM model, the out of plane bending rigidity of the beam elements should be related with

the weak inversion energy of the covalent bond. As shown in Figure 6, in a covalent bond OA subjected to an out of plane force Fz (inducing moment My), only one third of the inversion energy is developed as:

$$UMy = \frac{1}{3} V\omega = \frac{1}{6} k\omega \theta y^2 \quad (12)$$

Where Kω= 1.1 kcal/mol [33] is the bond inversion energy, Vω the inversion energy of the atom at O and Θy the bending angle.

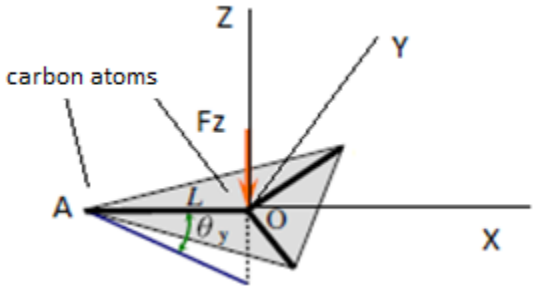

Figure 6: Out of plane loading of the covalent bonds

Combining equation (12) with (6), the out of plane bending rigidity is related with the force field inversion constant as:

$$k\omega = \frac{3\, EIout}{L} \quad (13)$$

Further combining equation (13) with (8), the relation between out of plane and in-plane rigidity is derived as:

$$Iout = \frac{k\omega}{3\, k\theta} Iin = 0.006\, Iin \quad (14)$$

It is evident from equation (14) that the out of plane rigidity in the mMSM is much smaller than the previous in the MSM approach. Combining equations (14) and (8), with the known force field constants and setting L=0.1421nm, A=0.001nm^2 and v=0.034 for the beam elements, the mechanical constants of the elements are calculated as:

$$E = 92649200 \frac{\text{pN}}{nm^2} \qquad G = 4.4801 \cdot 10^7 \frac{\text{pN}}{nm^2}$$

Where pN are pico Newtons chosen for numerical convenience. The rigidities are derived as:

$$Iin = 1.3436 \cdot 10^{-6} nm^4 \quad Iout = 8.0613 \cdot 10^{-9} nm^4 \quad J = 4.2638 \cdot 10^{-7} nm^4 \quad (15)$$

The mMSM model of a GS can afterwards be developed in ABAQUS, using Generalized Sections for the beam elements. Each beam finite element captures the phenomena in the smallest scale between the atoms, while the total frame model behaves like a shell in larger scales. Validation tests for such models include the tension test, for the calculation of the mechanical constants. A tension test of the finite element model, provides the Young's Modulus and the Poisson's ratio of the sheet, calculated at E=1.04TPa and v=0.0607, using the graphene interlayer spacing t=0.34nm as equivalent thickness. The tension test was conducted for a 22.1676x21.1676nm GS in the zig-zag direction, shown in Figure 7, which is homogenous enough to provide accurate results.

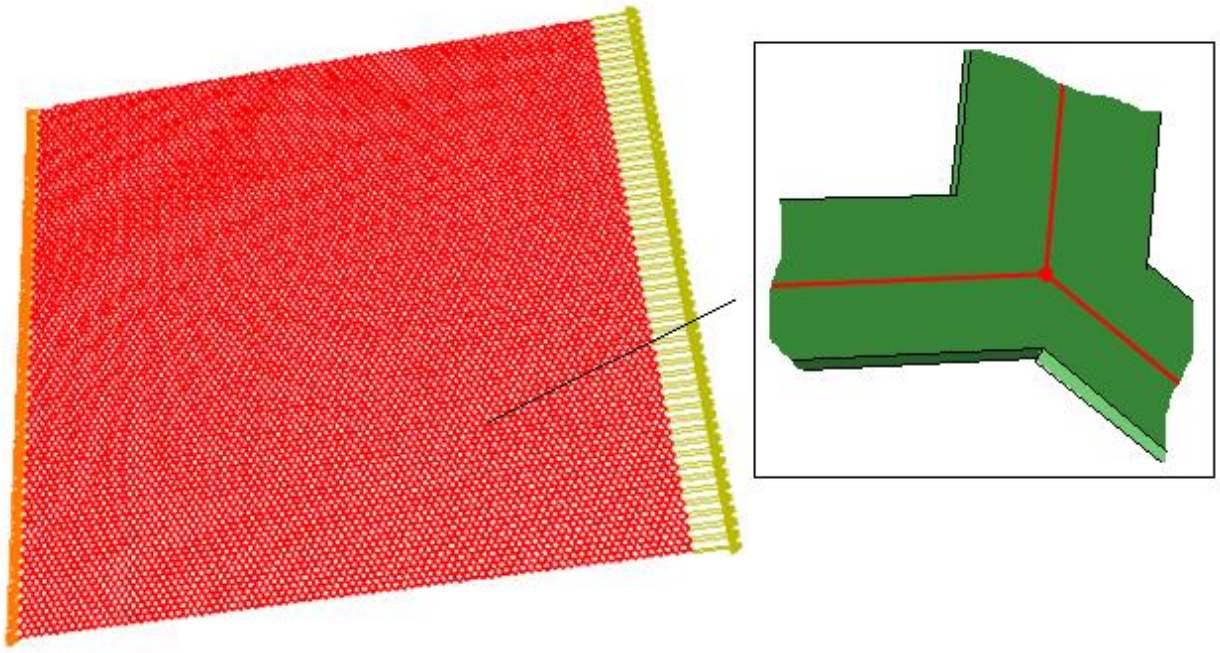

Figure 7: Tension Test for a 22.1676x21.1676nm GS in the zig-zag direction, modeled with the mMSM finite element approach

A not significant variation in the mechanical constants is observed in the armchair direction, which leads to fact that the GS can be regarded having isotropic membrane behavior, supported also by other studies [15]. The model size also has a slight effect, with an 88.67x84.66nm model having a calculated value of Young's modulus E=1.0369 TPa. Such variations are considered negligible, indicating that the mMSM frame model performs well in all sizes. However, even though the calculated Young's modulus of the GS is consistent with other studies [12,15,17,35,36], there has been much discussion about the calculated Poisson's ratio which is scattered in a wide range of 0.06 to 0.45. As stated by Baykasoglu and Mugan [35] who

applied the MSM method and calculated a value of v=0.063, there is lack of experimental studies about the Poisson's ratio. In the present work, the value of v=0.0607 which validates the mMSM model will be used, for all further simulations of the GS.

2.3 The Equivalent Shell Element of a Single Layer Graphene Sheet

In paragraph 2.2 the theoretical aspects behind the mMSM finite element model of GS were described. The mMSM approach leads to beam finite elements capturing the interatomic interactions in the smallest scale of a GS, while the mechanical behavior in larger scales is simulated by the equivalent frame model. Even though this multiscale simulation is computationally effective compared to atomistic simulations [17-20], the cost of analysis is still high when relatively large GS models are simulated. For example an mMSM model of a single layer graphene sheet (SLGS) of 44.33x42.33 nm, consists of 73000 beam elements. A model of 88.76x84.66 nm consists of 430000 beam elements, making even simple static loading conditions very computationally demanding. It is evident that simulations in the scales of micrometers with current mMSM models are very inefficient, if not impossible. The restrictions of size and time analysis of the mMSM method are dealt with further substitution of the beam frame, with an equivalent continuum element; which has already found application in the modeling of CNTs as an equivalent beam element (EBE) [21-23]. The process of finding the EBE of CNTs, shown in Figure8, involves simple loading tests for the calculations of the mechanical constants of the EBE.

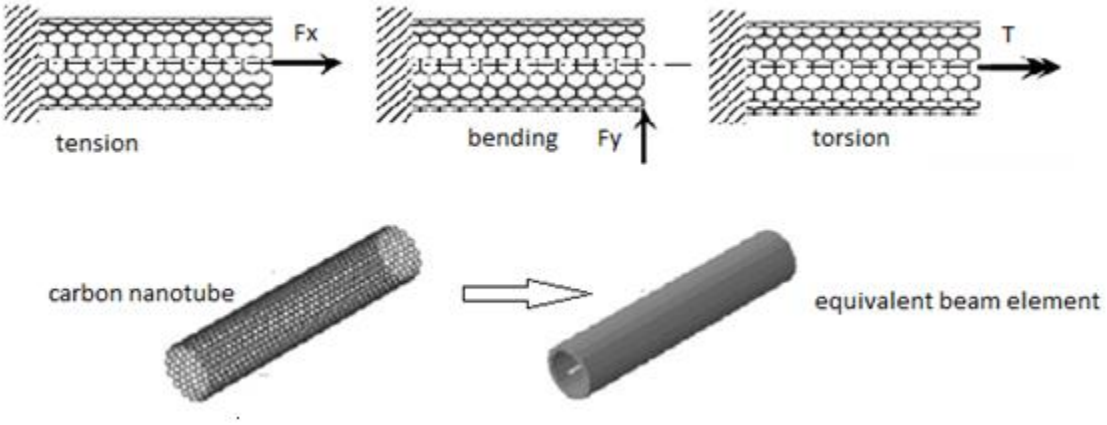

Figure 8: Mechanical tests leading to the Equivalent Beam Element of a carbon nanotube

The much lower element to volume ratio achieved via the EBE, makes possible the simulation of larger scale models and longer time spans, which are necessary for various simulations in the studies of nanocomposites. Along with the low computational cost, great accuracy is also provided with the EBE [21], both by means of mechanical behavior and retention of the original

dimensions of the model. The present work aims to find the equivalent shell element (ESE) of a SLGS in a similar way. While a CNT behaves like a beam, a SLGS is found to have a plate like behavior when subjected to out of plane loads. A frame structure for a rectangular SLGS of 11.08x10.58 nm with all edges clamped, subjected to an out of plane load of 6 pN at the middle, is shown in Figure 9.

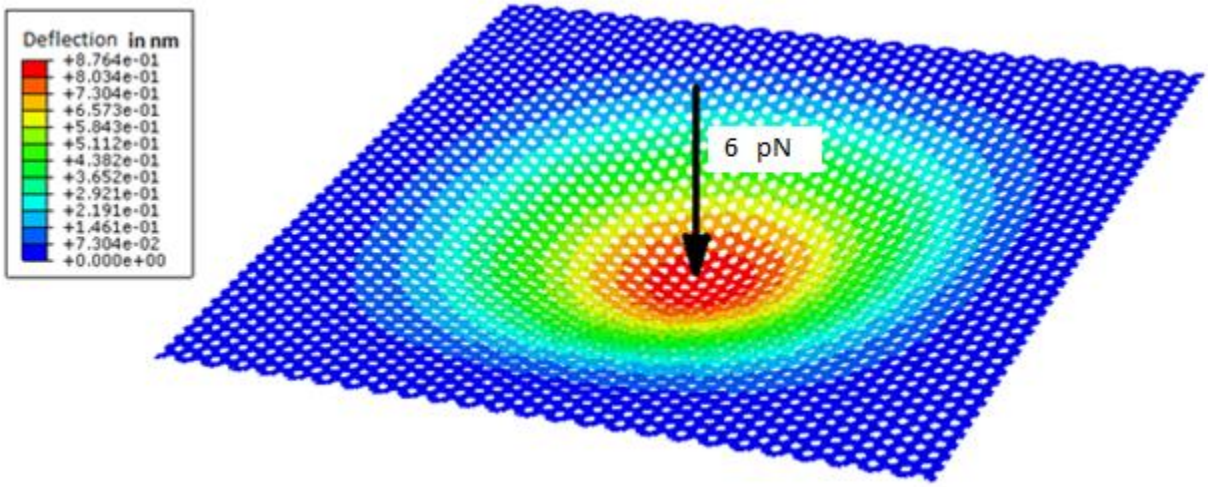

Figure 9: A rectangular 11.08x10.58 nm SLGS with all edges clamped, subjected to an out of plane 6nN load

The plate behavior shown in Figure 9, along with the membrane behavior observed in the tension tests leads to the fact that a SLGS behaves like a shell structure. Limited studies are currently available about modeling the plate behavior of a SLGS with equivalent plate elements [37,38], but no information is available about combined plate and membrane behavior in a single approach. Difficulty arises when searching for the equivalent shell due to the fact that an ESE would have to validate both the membrane and the plate behavior of the SLGS simultaneously. Bending tests indicate that the correct bending rigidity for a plate SLGS is much less than the rigidity obtained when using the membrane behavior mechanical constants E=1TPa and v=0.0607. In the present work a suitable approach addresses this issue, in terms of the uncoupled membrane and plate behavior in thin shells. If a SLGS is to be considered as a thin shell, meaning that its thickness is very small compared to its size and no shear stresses are developed, the stiffness matrix K of a shell finite element has uncoupled membrane and plate behavior according to:

$$K = \begin{bmatrix} Km & 0 \\ 0 & Kb \end{bmatrix} \qquad (16)$$

Where Km is the stiffness sub-matrix that corresponds to the membrane behavior of the shell and Kb the stiffness sub-matrix that corresponds to the plate behavior of the shell. Therefore, two equivalent continuum models are necessary, an equivalent membrane element (EME) and an equivalent plate element (EPE). A finite element solution of a SLGS with an ESE can afterwards be provided by equation (16). A representation of the degrees of freedom that correspond to membrane and plate finite elements with 4-nodded quadrilateral elements is shown in Figure 10.

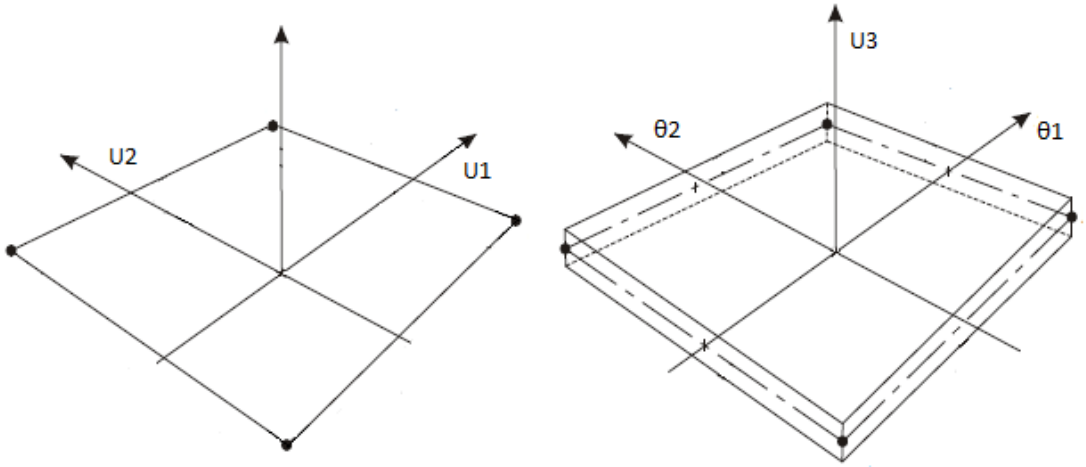

Figure 10: The degrees of freedom that correspond to 4-nodded quadrilateral membrane (left) and plate (right) finite elements

The EME physical properties are already known from the tension tests, as E=1TPa, v=0.0607 and thickness=0.34 nm, thus the Km finite element stiffness matrix can be directly formulated. For the derivation of the EPE properties, a thin plate finite element model of a SLGS is developed in MATLAB, aiming to provide an approximation of the EPE regarding the mMSM model as the exact solution. For the EPE to have consistency with the bending behavior of the mMSM model, certain constraints must be satisfied, such as equal strain energy and displacements when the same loading and boundary conditions are applied. With an EPE that validates the bending behavior of a SLGS in multiple size scales, the development of the ESE is completed as a computationally effective solution for the modeling of graphene. The EPE procedure is presented in paragraph 2.4.

2.4 The Equivalent Plate Behavior of Graphene

The method described in this paragraph can be regarded as a general method of deriving the EPE physical properties of a frame model. As stated in paragraph 2.3 the present work aims to

develop the EPE, which describes the bending behavior of the ESE of a SLGS. Considering the mMSM solution as the excact, a MATLAB optimization algorithm is applied in order to reach a solution that minimizes the error between the EPE and the mMSM model. Both models should be subjected to the same loading and boundary conditions. The loading test is chosen for a rectangular plate with all edges clamped, as shown in Figure 11. Constraints need to be applied in the algorithm for convergence to physical properties that validate the mMSM, for every other loading condition. The uniqueness of solution in structural mechanics, provided by the minimization of the potential energy, makes the strain energy a necessary constraint. The EPE also needs to be geometrically consistent, thus displacement constraints need to be applied. Therefore, assuming that the EPE exists and can be modeled with thin plate finite elements, the problem is formed in steps as following:

1. *Assume that an equivalent plate element of the frame exists*
2. *The plate element is modeled with thin plate finite elements forming the stiffness matrix K, force vector F and displacement vector U*
3. *Find the plate properties X by solving the optimization problem:*

$$Minimize f(X) = |Vframe - Vplate(X)|, where\ V\ \ is\ the\ \ strain\ energy$$

$$with\quad X = \begin{bmatrix} E \\ v \\ t \end{bmatrix}$$ *where E is the Young's Modulus, v the Poisson's ratio and t the thickness*

$$constrained\ \ \mathbf{by}\ \ g(X) = |\max(Uframe) - \max(Uplate(X))| = 0\ \ \mathbf{and}\ X \geq 0 \qquad (17)$$

The optimization problem in (17) can be further simplified by setting a constant value of v=0.0607 and thickness t to be geometrically consistent with the EME. This leads to the optimizer searching only for the Young's modulus E of the EPE. The equivalent thickness can afterwards be altered, and then calculate the new E by solving the plate rigidity equation D for the new thickness t:

$$D = \frac{Et^3}{12(1-v^2)} \qquad (18)$$

A summary of the process followed in the EPE method is depicted in Figure 11. The finite element equations and matrices used in the optimization algorithm can be found in many textbooks regarding the finite element method in solids [39,40]. In the present work, Kirchoff plate finite elements numerically integrated in MATLAB were used.

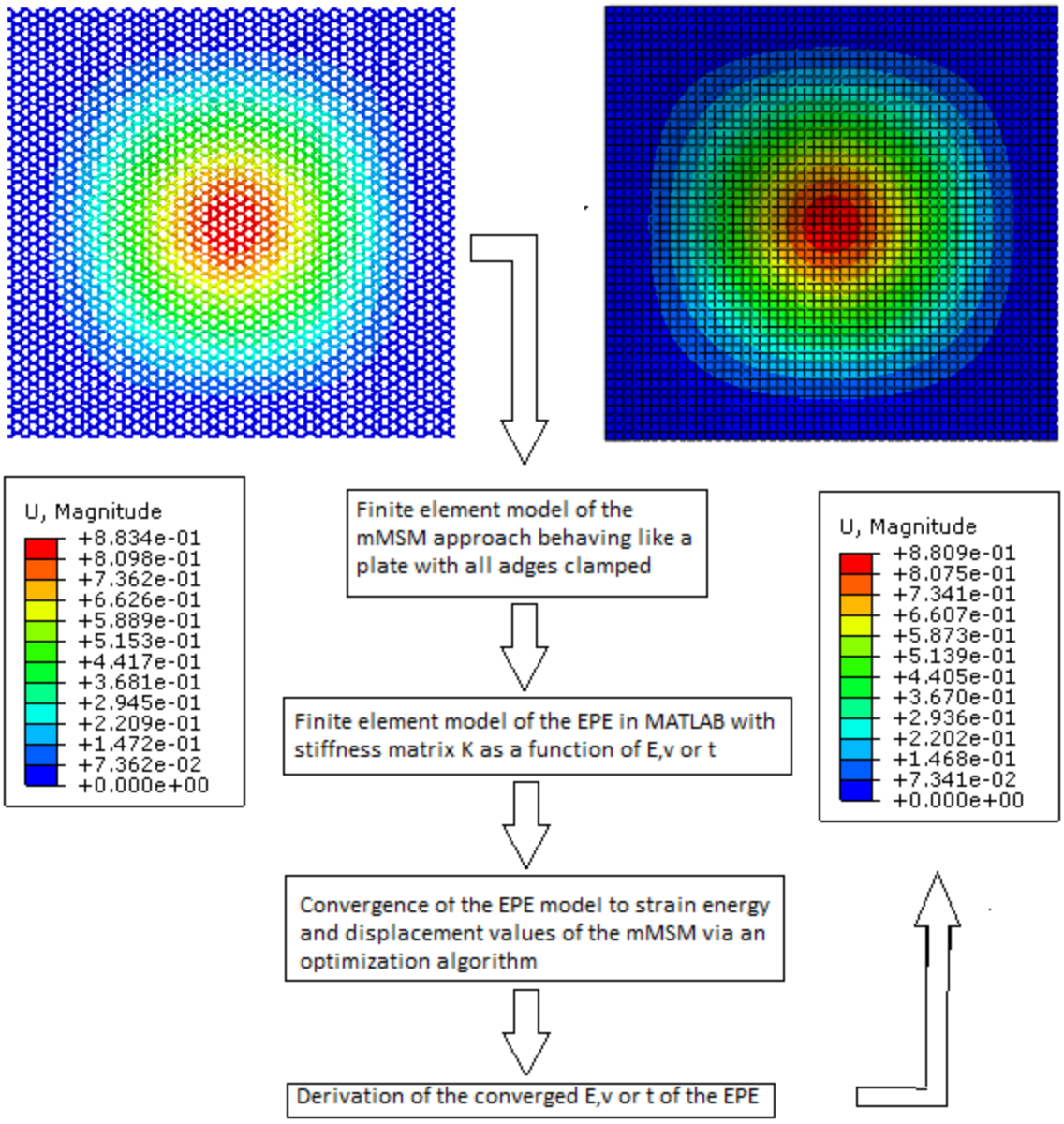

Figure 11: Summary of the process followed for the derivation of the EPE parameters

In the method described above, no assumptions were made about the shape of the lattice. Therefore, the EPE method can be applied in a frame model, regardless of lattice shape, provided that the frame behaves like a plate. How well is modeled the hypothetical EPE depends on the number of finite elements used. The necessary number of plate finite elements in (17), for the obtained E to be valid, can be determined by observing the effect of the mesh density on the Young's modulus of the EPE. In Figure 12, the graph of E versus the Number of plate elements is depicted for a 11.08x10.58 nm SLGS. A finite element mesh of 40x40 plate elements is adequately fine and converges to a solution of E=53412035928 pN/nm^2. The effect

of the size of the model used in the optimizer is also depicted in Figure 13; for various SLGS sizes modeled with 40x40 plate finite elements.

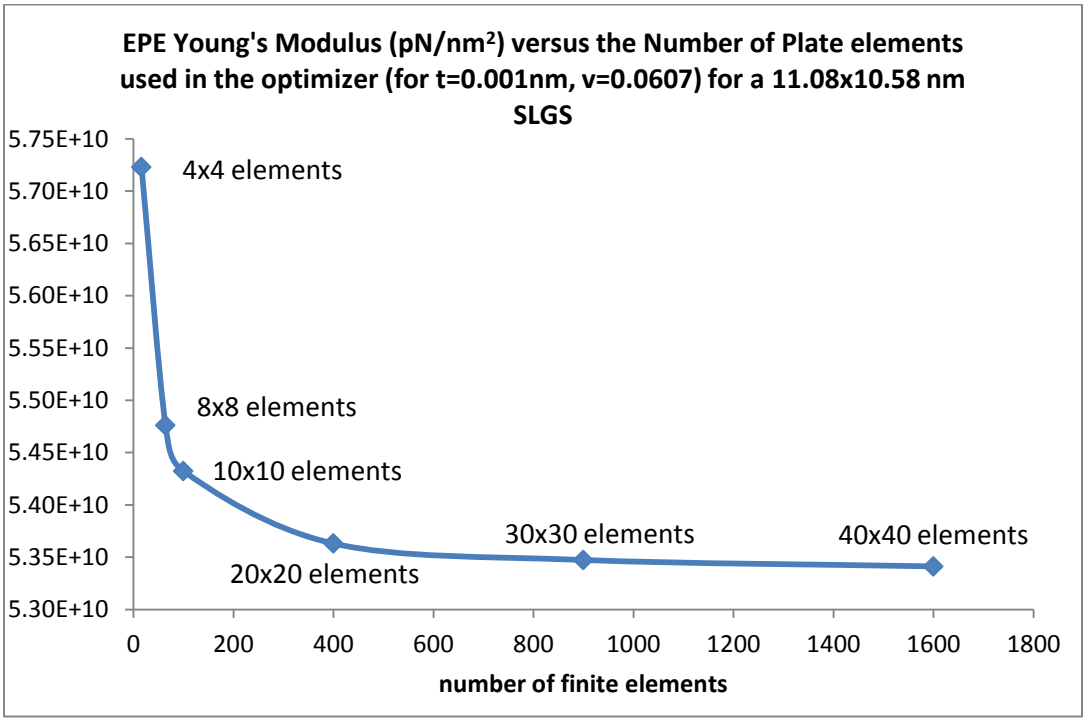

Figure 12: Dependence of the EPE Young's Modulus on the finite element mesh density

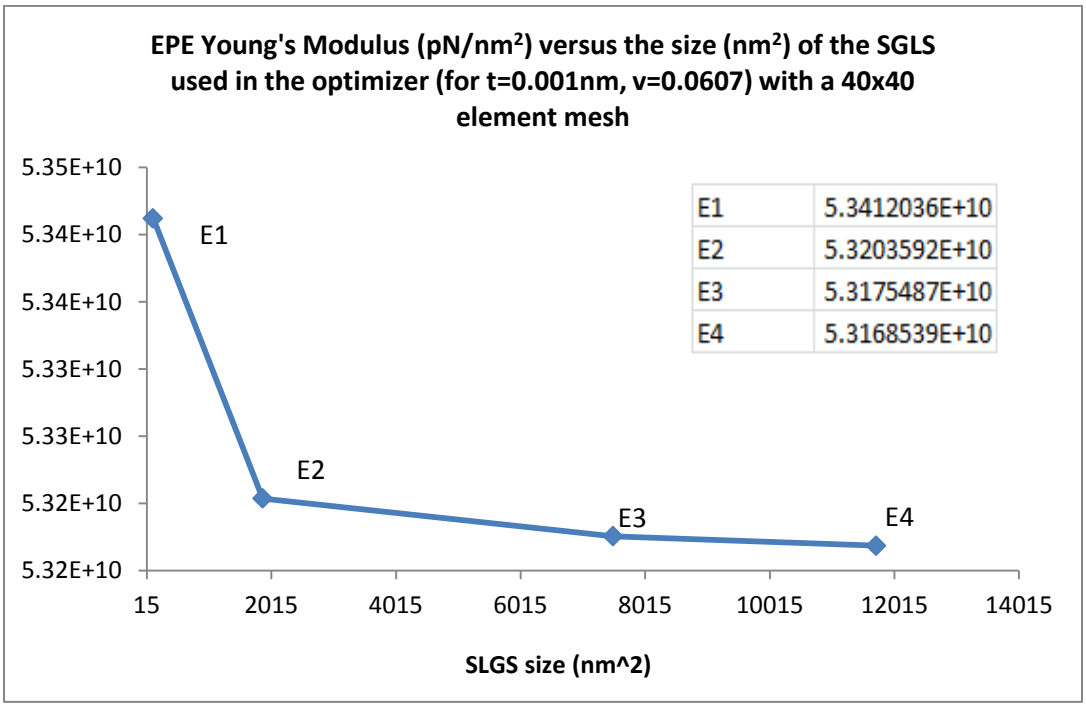

Figure 13: Dependence of the EPE Young's Modulus on the mMSM model size

A SLGS of 11722 nm^2 that corresponds to 105x111 nm, is homogenous enough to converge to the value of E=53168539247.1 pN/nm^2. The interesting observations from Figures 12 and 13 illustrate the sensitivity of the method to the finite element mesh density and the size of the model. A mesh of 40x40 elements is adequate, while the size of the model seems to slightly affect the results, with a maximum of 0.37% difference in E between models of over 100 times difference in terms of surface. Validation of the method would include also tests of an EPE with different loading and boundary conditions, in the same or different size scales. In Figure 14, the graph of the error in displacements and strain energy, versus the model size is depicted, for an EPE Young's modulus derived from the 11.08x10.58 nm SLGS. The loading and boundary conditions correspond to all edges clamped, with a concentrated load in the middle.

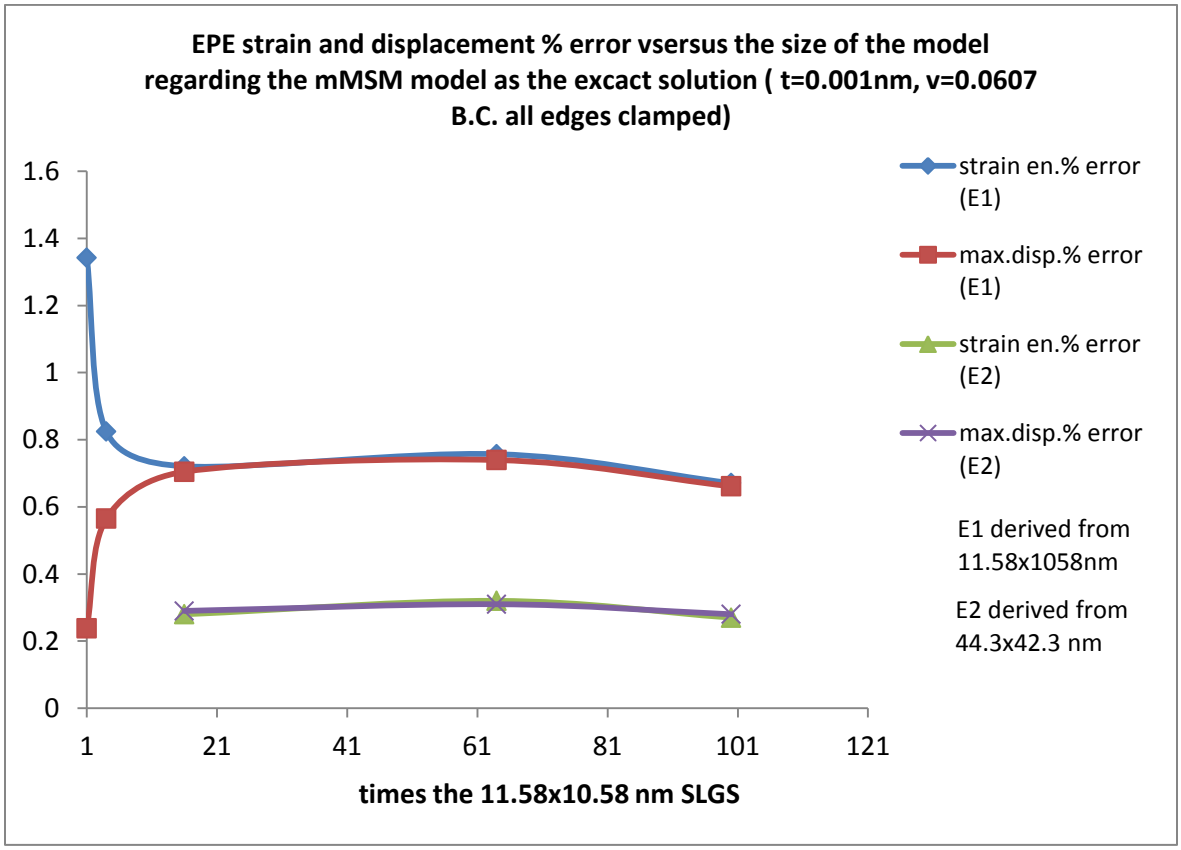

Figure 14: Strain and displacement % errors for EPE versus the size of the model

The very small error in displacements and strain energy reveals the great accuracy of the EPE, while the model shifts sizes. The strain energy and displacement error develop the same from a point up to 20 times (in terms of surface) the 11.58x10.58 nm SLGS; corresponding to a 44.3x42.3 nm SLGS. This is attributed to the higher homogeneity of the mMSM model as the size increases, behaving more like a plate. However, high accuracy is observed in all model sizes, with a bounded error growth, which is almost zero up to a 44.3x42.3 nm SLGS. Bending

tests with different boundary and loading conditions, such as an asymmetric loading shown in Figure 15, indicate errors of similar magnitude, below 1% in strain energy and displacements for all model sizes. The EPE therefore exists for a SLGS and can be modeled with plate finite elements.

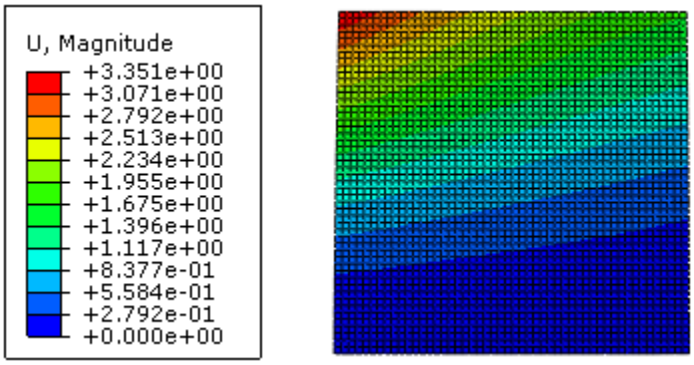

Figure 15: An asymmetric bending test with a concentrated force and one edge clamped for the EPE of a 44.3x42.3nm SLGS, modeled with 50x50 plate elements

Regarding the computational efficiency of the EPE, the graph of Figure 16 illustrates the effectiveness of the EPE as the size of the SLGS increases.

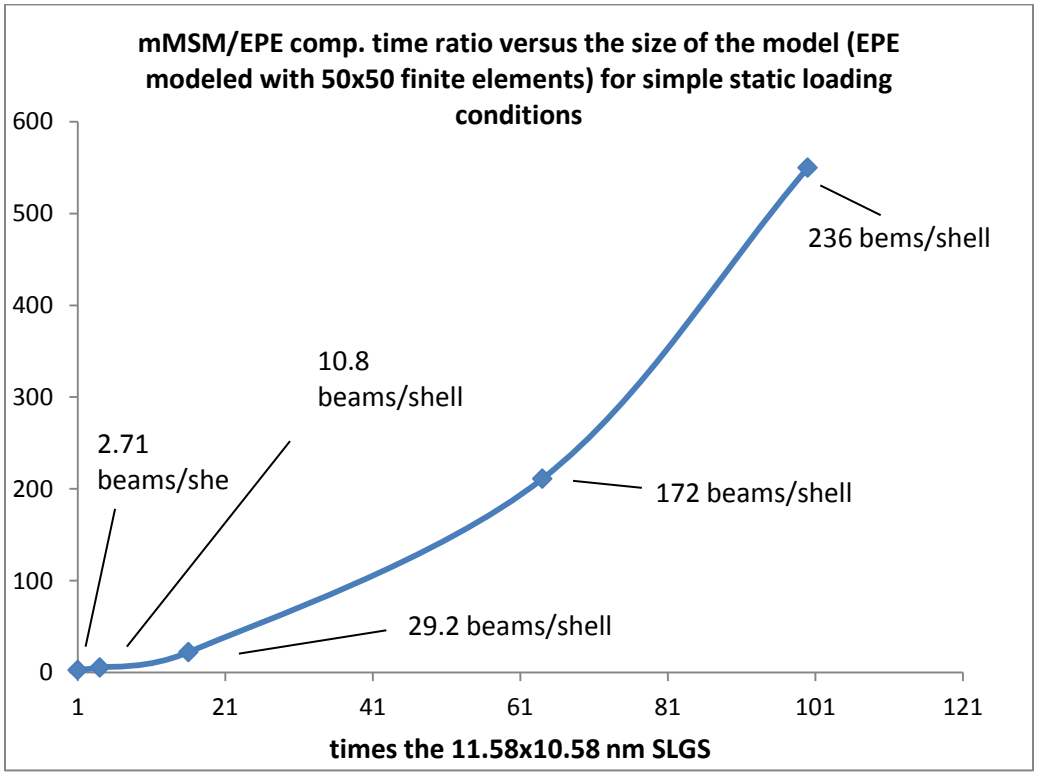

Figure 16: Computational time ratios achieved with the EPE

The EPE approach is found to be over 600 times faster than the original mMSM model for a SLGS larger than 100x100 nm, while the accuracy in terms of strain energy and displacements is kept over 99%. Therefore, the EPE approach makes possible accurate finite element simulations of SLGS in large size and longer time scales. The properties of the EPE are chosen as:

$$E = 1352.5 \ \frac{\text{pN}}{nm^2} \ \text{=1.352 GPa} \qquad t = 0.34 \ nm \qquad v = 0.0607 \qquad (19)$$

Where the E has been chosen as the converged value E4 regarding the model size (Figure 13), and afterwards recalculated for t=0.34 nm using (18). The values in (19) can be used for a SLGS in the scales of micrometers with over 99% accuracy, considering that the E in (19) has been obtained from a 105x111 nm SLGS which is highly homogenous and the error behaves as shown in Figure 14; with an almost zero growth for a homogenous SLGS as it shifts sizes (E2 values in Figure 14). The ESE of a SLGS can afterwards be formulated using (16) with finite elements, for the analysis of a SLGS in multiple scales.

3 The Finite Element Model of Graphene Reinforced Nanocomposites

3.1 The Interfacial Load Transferring Mechanism

The Interfacial Load Transferring Mechanism (ILTM) between the matrix and the filler has attracted a lot of scientific interest, due to its importance on the mechanical behavior and properties of nanocomposites. In a polymer matrix nanocomposite, while the carbon atoms in graphene interact through strong covalent bonds, graphene or CNTs interact with the matrix through weak Van der Waals forces [27,41]. Techniques known as functionalization [25,26] have been applied, in order to covalently bond carbon atoms with the polymer, greatly enhancing the ILTM stiffness and strength. Experimental studies in CNT reinforced composites (CNT-RC) [42] reveal a non-linear pull-out force-displacement relation when the interfacial strength (IS) values are exceeded. In the case of an ILTM based only on VDW forces, the IS values are relatively low, meaning that the stiffness of a GS-RC depends on the strain. Therefore, the correct modeling of a CNT-RC or a GS-RC has to take into account the effect of the ILTM. In a similar way, as in the analysis of graphene via the multiscale mMSM model, the ILTM has been modeled with equivalent continuum structural mechanics techniques in nanocomposites. Three main approaches have been proposed in finite element simulations for the filler-matrix interactions, a friction or shear lag model [21,27,43], a non-linear spring model [41,44] and a cohesive zone simulation [30,45]. In the present work, a friction model cannot be directly applied due to the absence of shear stresses in the thin ESE. In addition, a non-linear spring model requires the simulation of the GS with beams, as the filler-matrix atom

interactions are modeled directly with spring elements that represent Lenard-Jones potentials. On the other hand, a cohesive zone simulation defines a traction-separation law between surfaces and can be used between the ESE and the matrix. Analytical expressions for a cohesive law in a GS-RC have been proposed based on a Lenard-Jones potential [46]. Also, pull-out molecular dynamics simulations [47] in a GS-RC reveal a similar behavior, suggesting [48] a cohesive zone for a multiscale finite element simulation. Therefore, the definition of a cohesive zone that follows a traction-separation law is applied in the present work for the modeling of the ILTM. A traction-separation law typically defines the traction vector t that is developed between two surfaces, as a function of their separation δ:

$$t = \begin{bmatrix} tn \\ ts \\ tt \end{bmatrix} = \begin{bmatrix} Knn & Kns & Knt \\ Kns & Kss & Kst \\ Knt & Kst & Ktt \end{bmatrix} \begin{bmatrix} \delta n \\ \delta s \\ \delta t \end{bmatrix} \qquad (20)$$

Where n, s and t correspond to the normal, shear1 and shear2 directions respectively, as shown in Figure 17, while the K coefficients correspond to stiffness. The relation in (20) provides a fully coupled traction-separation behavior. In the present work, the simplest decoupled form is applied, keeping as non-zero only the diagonal terms Knn, Kss and Ktt. Generally the stiffness coefficients are constant values leading to a linear response prior to damage, which is initiated according to a criterion. Generally, three damage modes as shown in Figure 17 may occur.

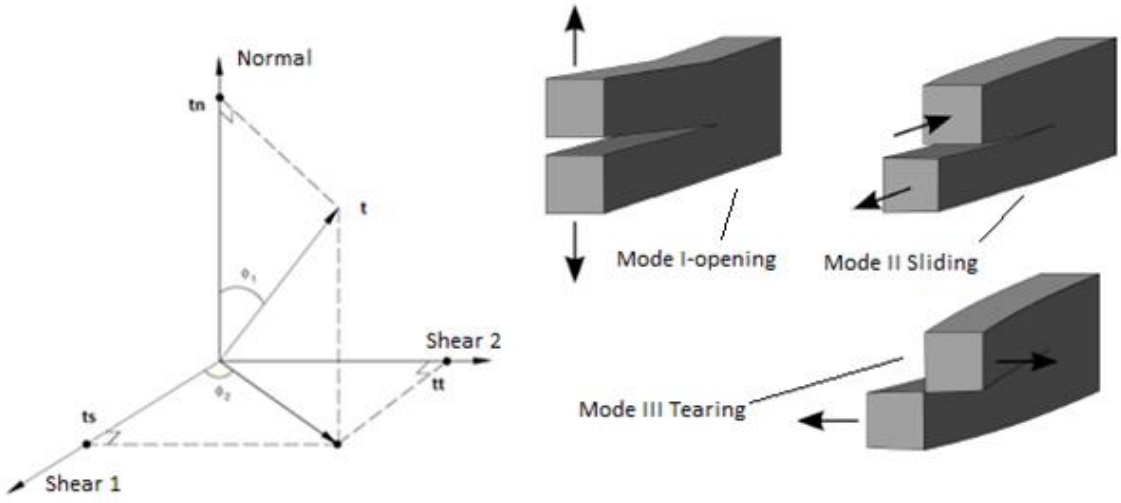

Figure 17: Left the Traction vector components and right the fracture modes

The criteria available for the damage initiation are based on maximum traction or maximum strain. In the present work, the damage initiation is assumed to occur when one or more of the traction components reaches the maximum value. Therefore the maximum nominal stress criterion can be represented as:

$$Max\left(\frac{tn}{tnmax}, \frac{ts}{tsmax}, \frac{tt}{ttmax}\right) = 1 \qquad (21)$$

Where tnmax, tsmax and ttmax represent the maximum values for undamaged response. Once damage is initiated, the cohesive stiffness is degraded according to a damage evolution law. A damage variable D is introduced, representing the overall damage with the value of D=0 for no damage and D=1 for maximum damage where no traction occurs. The contact stress components are calculated as functions of the damage variable D according to:

$$tn \begin{cases} tn = (1-\mathrm{D})\bar{tn}, & \bar{tn} \geq 0 \\ \bar{tn} & otherwise \end{cases}$$

$$ts = (1-\mathrm{D})\bar{ts}$$

$$tt = (1-\mathrm{D})\bar{tt} \qquad (22)$$

Where $\bar{tn}$, $\bar{ts}$ and $\bar{tt}$ are the tractions calculated by the elastic traction-separation response without damage in (20). The values of D develop dependent on the chosen damage evolution model. Typically the damage evolution can be based either on the fracture energy or the effective displacement and have a linear or exponential softening law. Modeling of failure depended on mix-mode condition laws can also be simulated. This general approach to the damage evolution could be used in every type of ILTM in a GS-RC, covalently bonded or not. In the present work we assume that the damage evolution in the GS-RC is based on effective displacements, is not depended on a mix-mode law and the stiffness degrades linearly. The effective displacement δm is expressed as a combination of the separations in each direction as:

$$\delta m = \sqrt{\delta n^2 + \delta t^2 + \delta s^2} \qquad (23)$$

The damage variable D degrades linearly following the expression:

$$\mathrm{D} = \frac{\delta_m^f\left(\delta_m^{\max} - \delta_m^0\right)}{\delta_m^{\max}\left(\delta_m^f - \delta_m^0\right)} \qquad (24)$$

Where δ_m^f, δ_m^0 and δ_m^{max} are the separations at complete failure, damage initiation and loading history maximum respectively. . A representative traction-separation curve is shown in Figure 18. The total plastic displacement $\delta_m^f - \delta_m^0$ when complete failure occurs is an input parameter for this damage simulation.

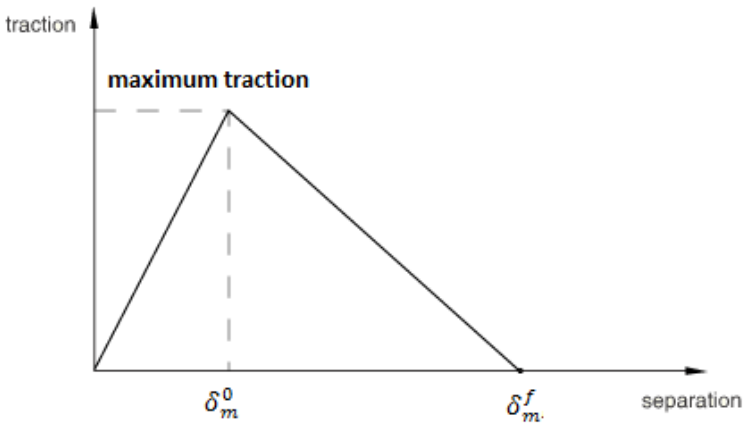

Figure 18: A Linear traction-separation response and damage evolution

Currently, uncertainty about the ILTM behavior and thus for the input parameters in (20,21,22) exists, with limited data available. However they could originate from accurate experimental data or molecular dynamics simulations designed for the present multiscale purpose. The table in Figure 19 summarizes traction values between the filler and the matrix with Vdw interactions, reported from molecular dynamics simulations.

Reported by	Loading Conditions	Maximum Shear Traction observed	Maximum Normal Traction observed
Zhang [47]	Pull-out of Flat SLGS in polyethylene	-	503.4 MPa
Liu [48]	Pull-out of Flat SLGS in polyethylene	112 Mpa	-
Awasthi [49,50]	Normal and Shear Mode separation of SLGS in polyethylene	108.276 Mpa	170.616 Mpa

Figure 18: Traction values observed in various molecular dynamics simulations of GS-RC with Vdw matrix-filler interactions

Various model parameters that affect the results in a molecular dynamics simulation, such as the size of the model are reported by Awasthi [50]. The input parametes of maximum interatomic matrix-filler distance, traction or force and stiffness, could be regarded as atomic scale parameters in a non-linear spring model. On the other hand, in the present work of the ESE model, as in the friction or shear-lag approach of the EBE model, the cohesive zone is modeled in a larger scale. Thus, differences exist with the non-linear spring models suggesting a 0.85 nm [41,44] as maximum separation distance for Vdw interactions, while friction or shear-lag models do not allow any separation in the multiscale before failure [21,27,43]. The latter consequently correspond to very high values in the cohesive stiffness in (20) and no separation

allowed after the IS values are reached. An equivalent continuum cohesive zone model originating from the non-linear springs, could be proposed as future work. In the present work, the effect of the parameters in (20,21,22), on the multiscale mechanical behavior of the SLGS-RC is investigated for different values, with comparison to the other approaches for the ILTM. The numerical results of the SLGS-RC are presented in chapter 4.

3.2 The Representative Volume Element of Graphene Reinforced Nanocomposites

A representative volume element (RVE) as defined by R.Hill [51] is a sample that is entirely typical of the whole structure on average. Analysis with RVEs is the dominant method in composites and nanocomposites, both with analytical methods and numerical approaches. For CNT-RC different RVE geometries [52] have been used to calculate the mechanical properties. However the most common RVE in GS-RC and CNT-RC is of rectangular shape. Therefore in the present work a rectangular RVE is developed, where the SLGS is embedded in a polymer matrix. For all the RVE simulations the commercial finite element software ABAQUS is used. Linear 3-D solid elements can be used for the matrix polymer, while thin shell elements must be used for ESE, shown in Figure 19. The ESE can either be modeled with a custom finite element, with uncoupled membrane and plate behavior that have different mechanical constants, or by stacking thin shell and membrane elements. Both approaches lead to a stiffness matrix in (16) as described in paragraph 2.3.

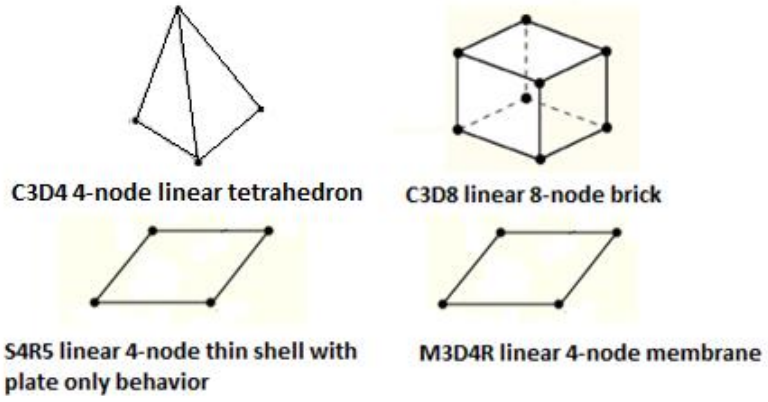

Figure 19: The finite elements used in ABAQUS for the SLGS-RC model

If the ILTM is not to be considered, meaning that the interface does not fail (perfect bonding), embedded element constraints can be applied directly between the ESE and the matrix. Information about the embedded element techniques can be found in the CNT-RC finite element simulations by D.Savvas [21,27]. This technique is generally simple and avoids

complicated discretization, while it can be used both for straight and wrinkled SLGS. A typical representation of an embedded SLGS in a nanocomposite matrix is shown in Figure 20.

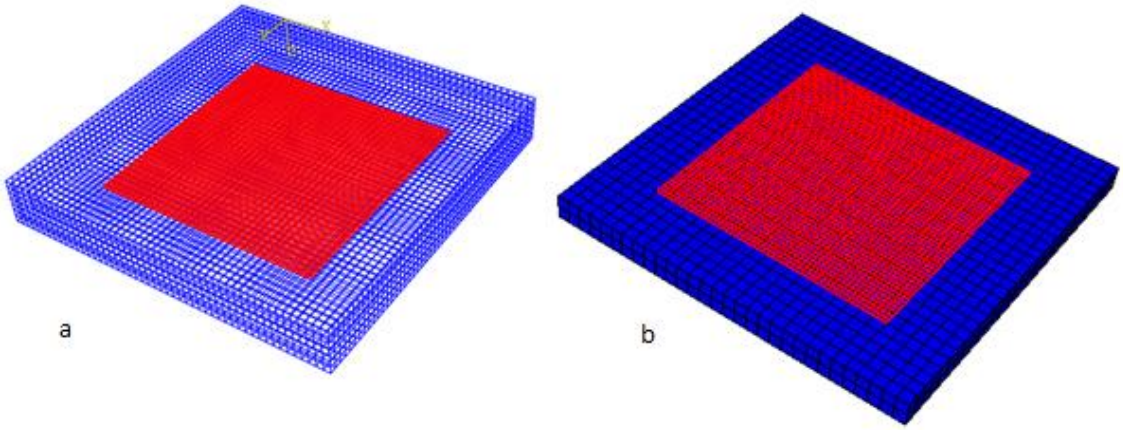

Figure 20: An example of a RVE for a SLGS-RC with finite element discretization in ABAQUS, a) using embedded element constraints, b) symmetric part of the RVE

For the consideration of the ILTM by a cohesive zone simulation as described in 3.1, ABAQUS offers two similar approaches, modeling with cohesive finite elements or modeling via a cohesive surface interaction. Cohesive elements [53] are regarded as special purpose elements that can have almost zero thickness, with a constitutive response defined in terms of traction versus separation. Previous applications include delamination and debonding analysis, both for composite [28-29] and nanocomposite [30] materials. Finite element formulations for cohesive elements can be found in the work of Davila and Camanho [54], who proposed a model for the problem of skin/stiffener debonding and delamination analysis; originally introduced by Krueger [55]. The skin/stiffener setup under tension, shown in Figure 21, presents a direct similarity with the symmetric RVE of a SLGS-RC shown in Figure 20.b.

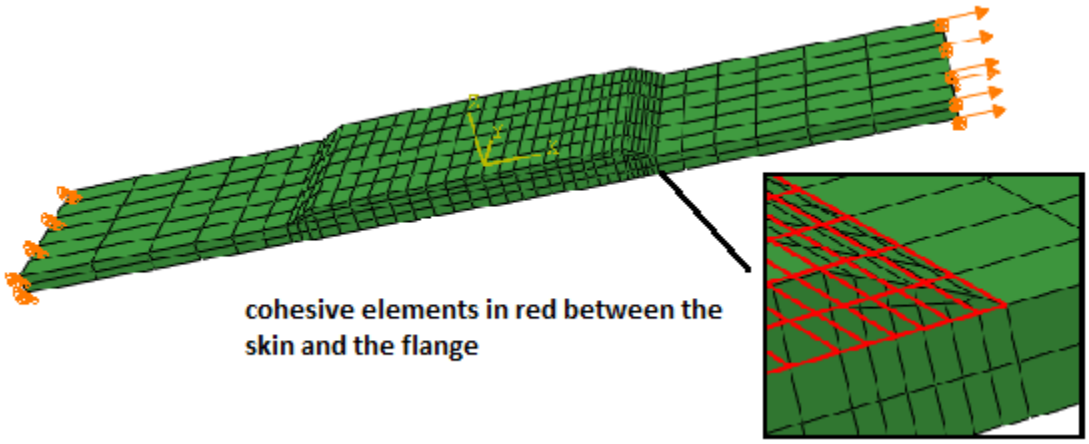

Figure 21: Skin/stiffener under tension with cohesive elements in the interface

A cohesive surface interaction on the other hand, avoids the use of special purpose elements, while the traction-separation law is imposed directly with a master-slave surface pair interaction. This approach is usually more computationally demanding, however it can be more flexible, as it can be applied instantly on any surface pair. Both approaches are expected to present similar results, with slight differences attributed to the dimensionless nature of surface interactions, compared to the small thickness of the cohesive elements. In addition, both approaches may present severe convergence issues, so ABAQUS has built in viscosity effects [56] for the damage propagation. Considering the modeling of wrinkled SLGS-RC with random geometrical defects, a special grid generator algorithm was developed in MATLAB. In the present work, randomness was implemented in a periodic form, assuming that the waves on a SLGS can be expressed as a function of trigonometric series with random initial phases. Generally, the random waves can be decomposed into high and low frequency components with different amplitudes. Therefore, the parameters of random defects on the mechanical behavior of the nanocomposite can be simulated. Figure 22 shows examples of randomly generated wavy SLGS, using different wave frequency parameters.

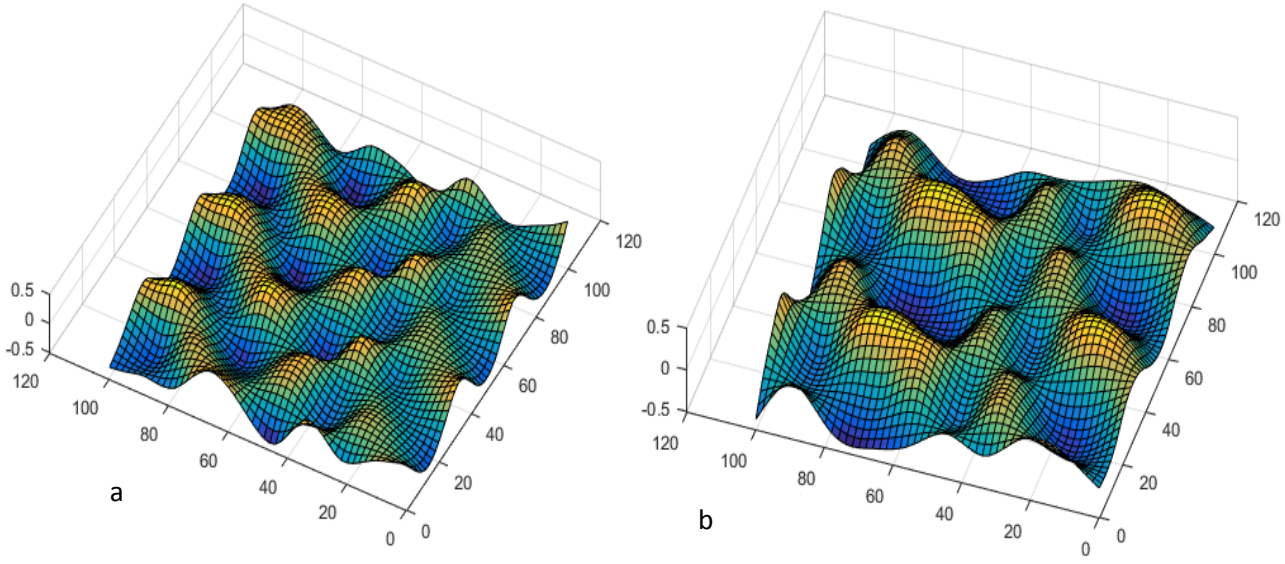

Figure 22: Randomly generated wavy 100x100nm SLGS, a) a relatively high frequency wave, b) a low frequency wavy

4 Numerical Results and Discussion

In the present chapter, the numerical results of the effect of the ILTM and wrinkles on the mechanical behavior of the SLGS-RC are presented and discussed. The general indicator for strain dependent mechanical behavior is the function of stiffness enhancement with respect to strain. The ESE approach can afterwards be validated by comparing results from other nanocomsite simulations. Conclusions are presented in Chapter 5.

4.1 The Effect of the Interfacial Stiffness

The effect of the interfacial cohesive stiffness (CS) (20) between the SLGS and the matrix, on the Young's Modulus of the nanocomposite, is presented in the following graph in Figure 23. The RVE is reinforced with a volume fraction of 0.75% graphene. The matrix consists of a linear 2GPa polymer and perfect bonding between matrix and filler is assumed, no damage is simulated for the polymer either.

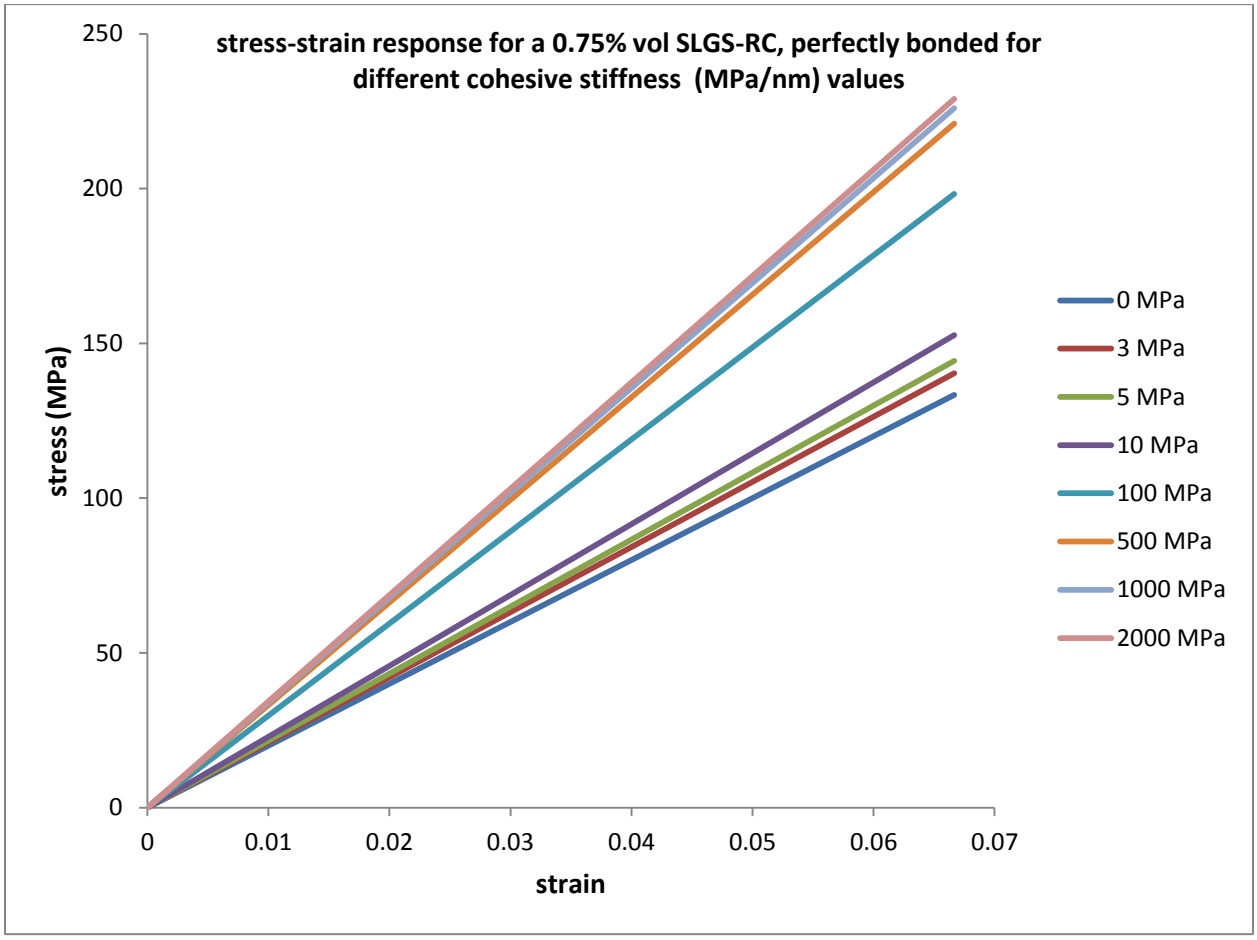

Figure 23: The effect of the interfacial cohesive stiffness on the Young's Modulus of the SLGS-RC with perfect bonding assumed

The percentage of the Young's Modulus enhancement with respect to CS is also presented in the following graph of Figure 24. It is evident that CS values over 1000 MPa/nm do not contribute significantly to stiffness enhancement.

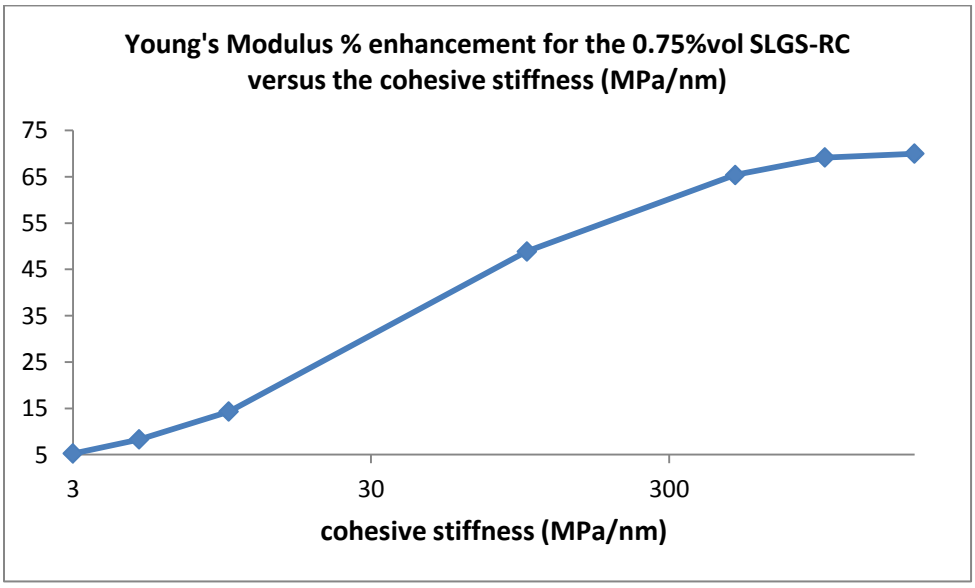

Figure 24: Young's Modulus enhancement for a perfectly bonded nanocomposite as function of cohesive stiffness

In addition, a high CS leads to small separations and different traction distributions arise in the interface. The values would of course depend on the matrix-filler bonds and the scale of the simulations as was stated in 3.1. The calculation and evaluation of these parameters is out of the scope of this work. However, as the ESE model is intended for large scale simulations, high CS could be used in a similar way as in conventional composites.

4.2 The Effect of the Interfacial Damage Evolution

The failure parameters of the ILTM discussed in 3.1 are the damage initiation and damage evolution of the traction separation law. We consider the effect of the ILTM damage evolution in a mean force-displacement response, similarly as the skin/stiffener under tension in Figure 21. The test RVE is of rectangular shape with dimensions of 150x150x20nm and consists of a 0.75%vol SLGS-RC. The damage evolution parameter is defined as the maximum plastic displacement (mpd) with linear degradation (24). Figure 25 shows the force-displacement curves for different bond cut-off separations. In Figure 26 and 27, snapshots of the nanocomposite as the delamination occurs are depicted. The results present direct similarity with the skin/stiffener delamination test [54]. A pull-out finite element test could be proposed

as future work, to derive the ILTM damage propagation parameters from pull-out molecular dynamics or experimental test data.

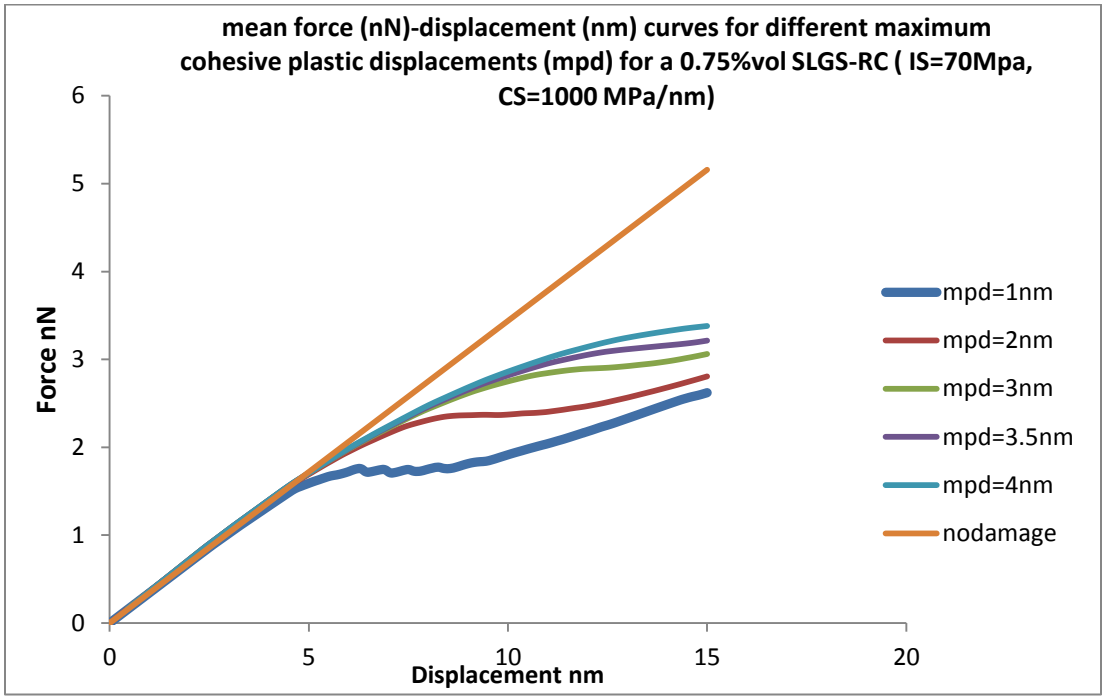

Figure 25: The effect of the ILTM maximum cohesive plastic displacement on a mean tensile force-displacement response

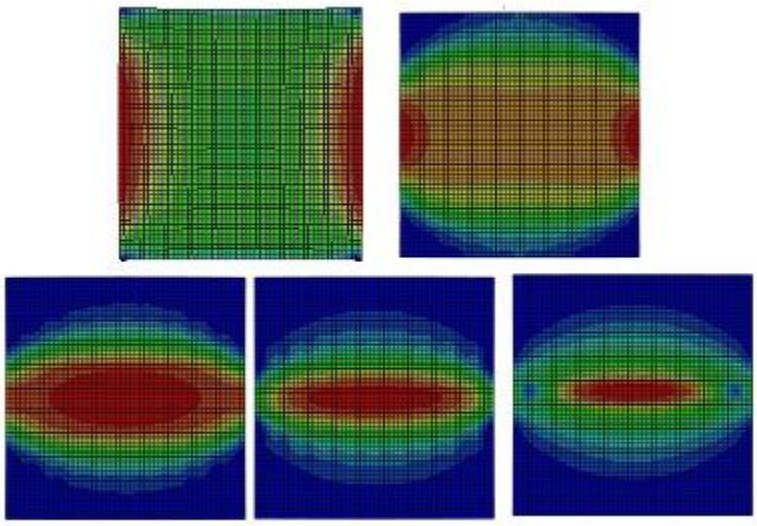

Figure 26: Snapshots of the mises stress distribution on the SLGS of nanocomposite corresponding to the force-displcacement curve of Figure 25 for mpd = 1nm. Bright areas indicate high stress, while dark areas indicate low stress as delamination propagates

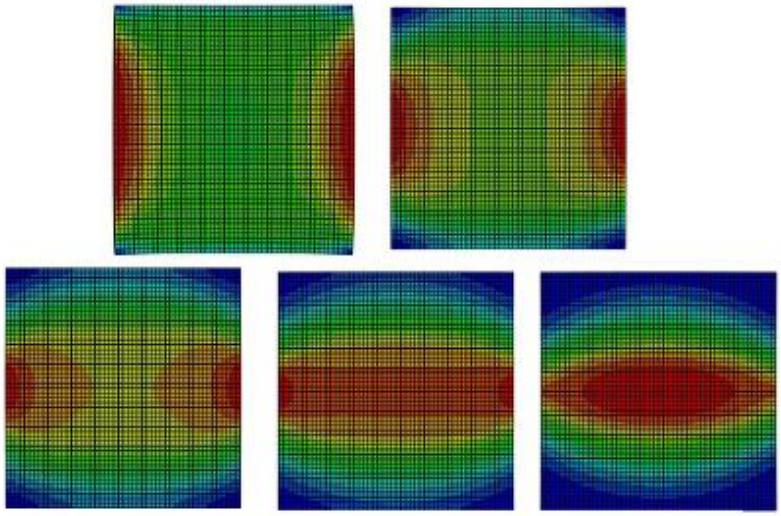

Figure 27: Snapshots of the mises stress distribution on the SLGS of nanocomposite corresponding to the force-displcacement curve of Figure 25 for mpd= 4nm. Bright areas indicate high stress, while dark areas indicate low stress as delamination propagates

For the lowest allowed plastic displacement, delamination in a large area is observed in Figure 25, with a resultant force close to the pure polymer. Therefore, the Young's Modulus of the nanocomposite is directly affected by the damage evolution parameters. A stress-strain response for the nanocomposite and the Young's Modulus % enhancement is depicted in Figures 28 and 29 respectively.

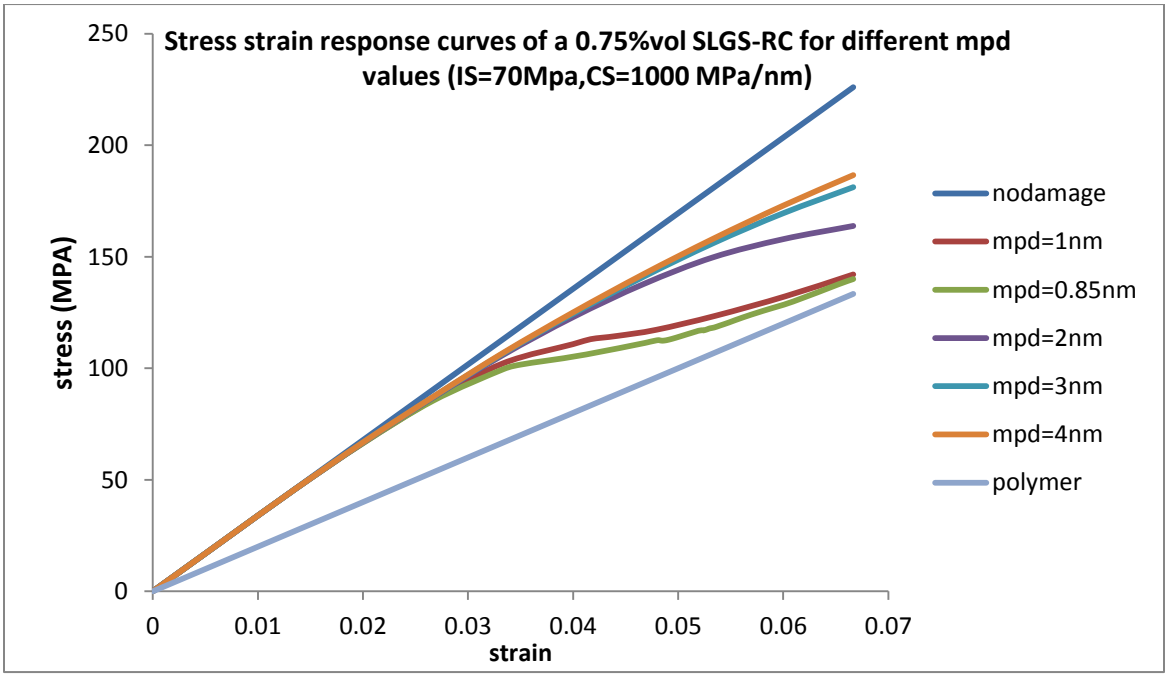

Figure 28: Stress-strain response of a SLGS-RC with ILTM damage simulation

The direct impact of the ILTM damage evolution on the stiffness enhancement, results in a strain dependent Young's modulus of the nanocomposite. The non-linear spring GS-RC [41] and CNT-RC [44] finite element models presented similar strain dependent Young's Modulus curves.

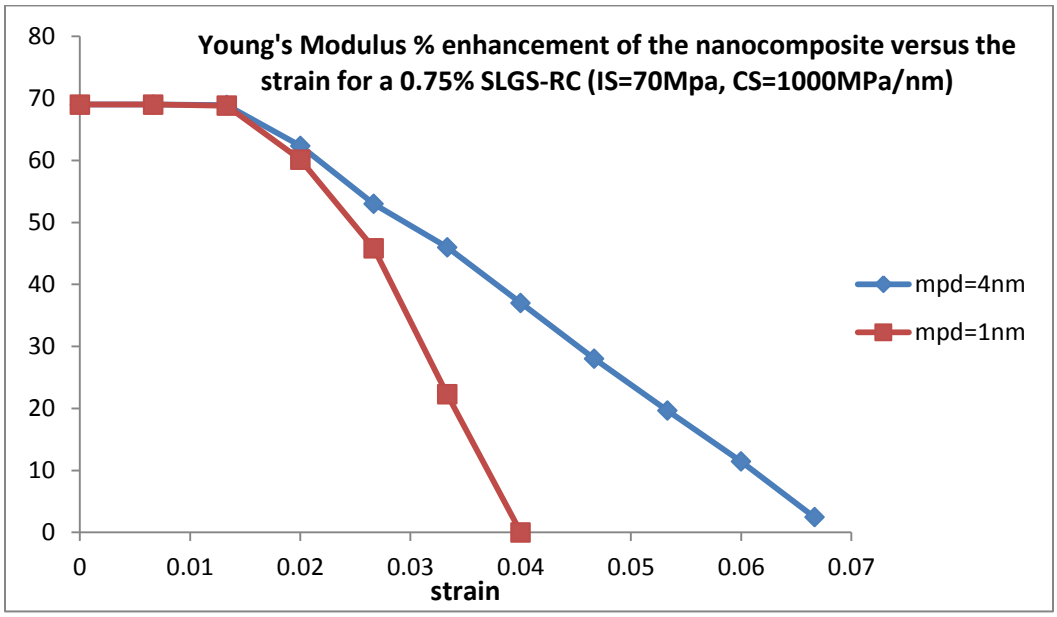

Figure 29: Dependence of SLGS-RC Young's Modulus enhancement on the strain

Regarding the mechanical behavior in cyclic loading conditions, assuming that damaged bonds can be regenerated the stress-strain response is depicted in Figure 30. Similar hysteresis loops have been presented in CNT-RCs [21,27].

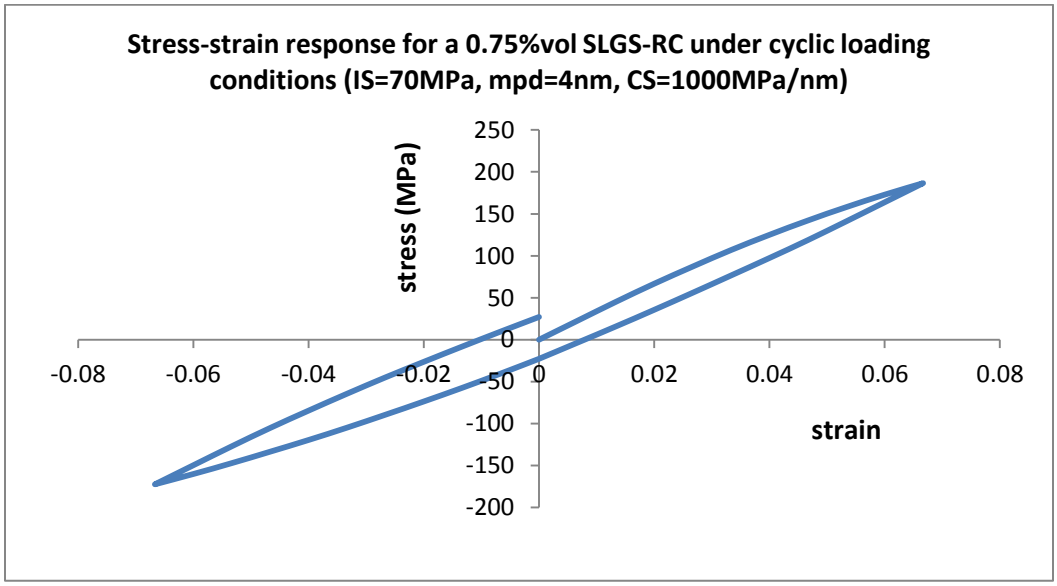

Figure 30: Stress-strain response of the SLGS-RC under cyclic loading conditions

4.3 The Effect of the Interfacial Strength

The effect of the interfacial strength on the mechanical behavior is depicted in the graph of Figure 31. The same maximum stress has been in assumed for all traction directions (21). Higher stiffness enhancement for greater interfacial strength values is obvious, and of course expected, as it has been highlighted in all of the CNT-RC or GS-RC studies. Figure 32 presents the stiffness enhancement as a function of strain.

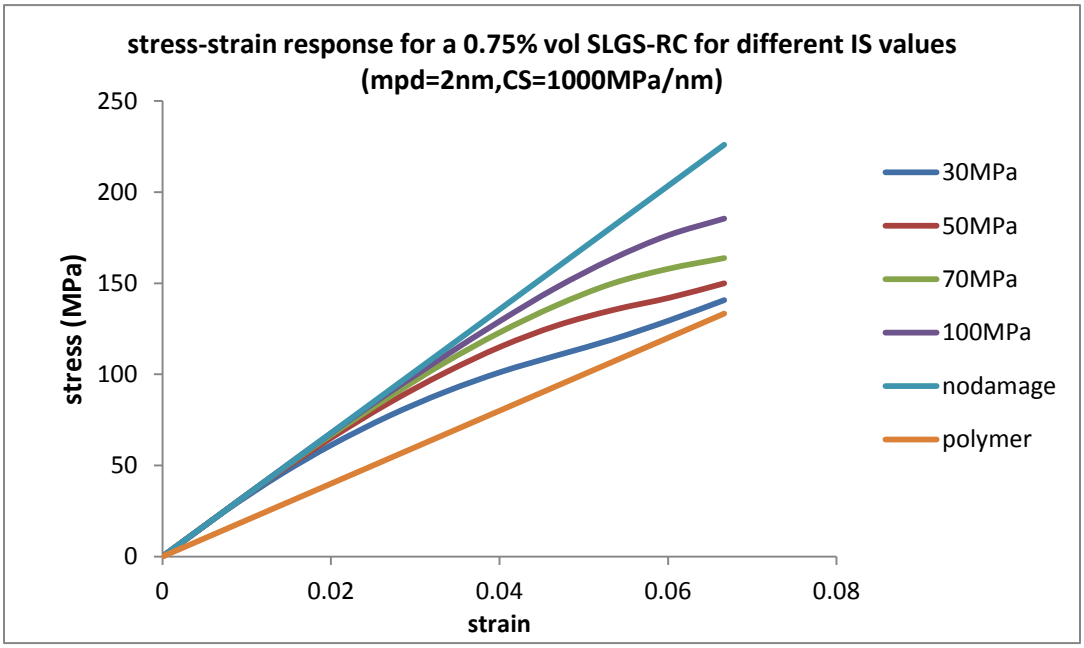

Figure 31: The effect of the interfacial strength on the stress-strain response of the SLGS-RC

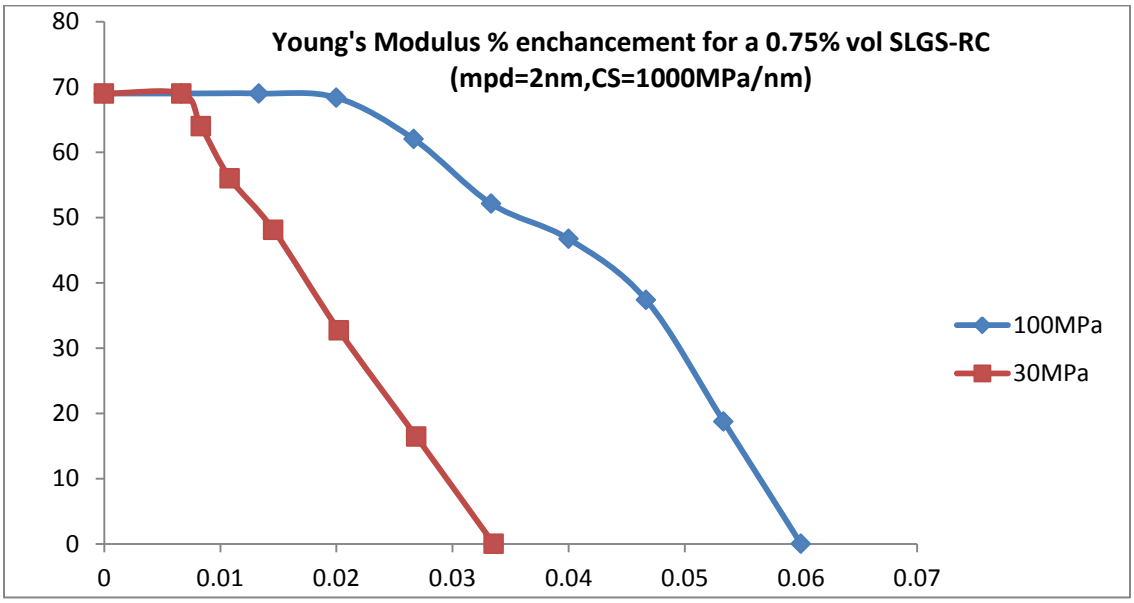

Figure 32: Young's Modulus of the SLGS-RC as a function of strain for different cohesive strength values

Assuming a relatively more ‘’brittle’’ bond with a maximum mpd=1.5 nm, the effect of the IS on the damping behavior can be studied, regarding the hysteric loop observed in the cyclic loading of Figure 30. Half of the stress-strain cycle is depicted in Figure 33 for better visualization of the hysteresis that occurs, due to bond failure and regeneration.

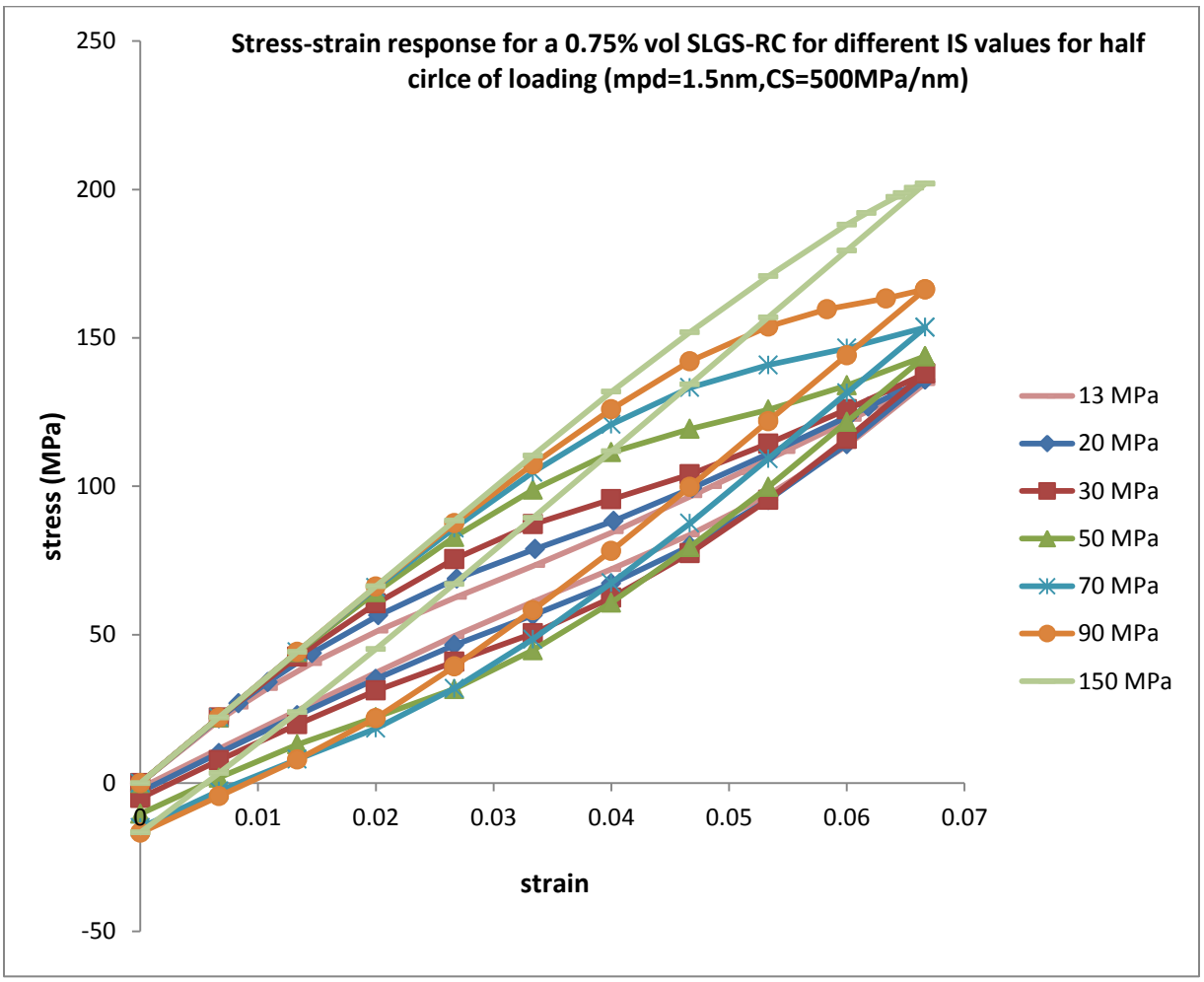

Figure 33: Stress-strain response for half cycle of loading with respect to different IS values

It can be seen that increasing the IS values, leads to larger dissipated energy area and also to higher maximum stress as was expected. However, very high values of IS, over 90 MPa initiate a reduction in dissipation area due to fewer bonds failing in the interface. The loss factor η for hysterical damping in one circle of loading can be calculated as:

$$\eta = \frac{D}{\pi U}$$

Where D is the dissipated energy area and U the energy stored during loading. Figure 34 depicts the graph of the loss factor with respect to different IS values for a full loading circle.

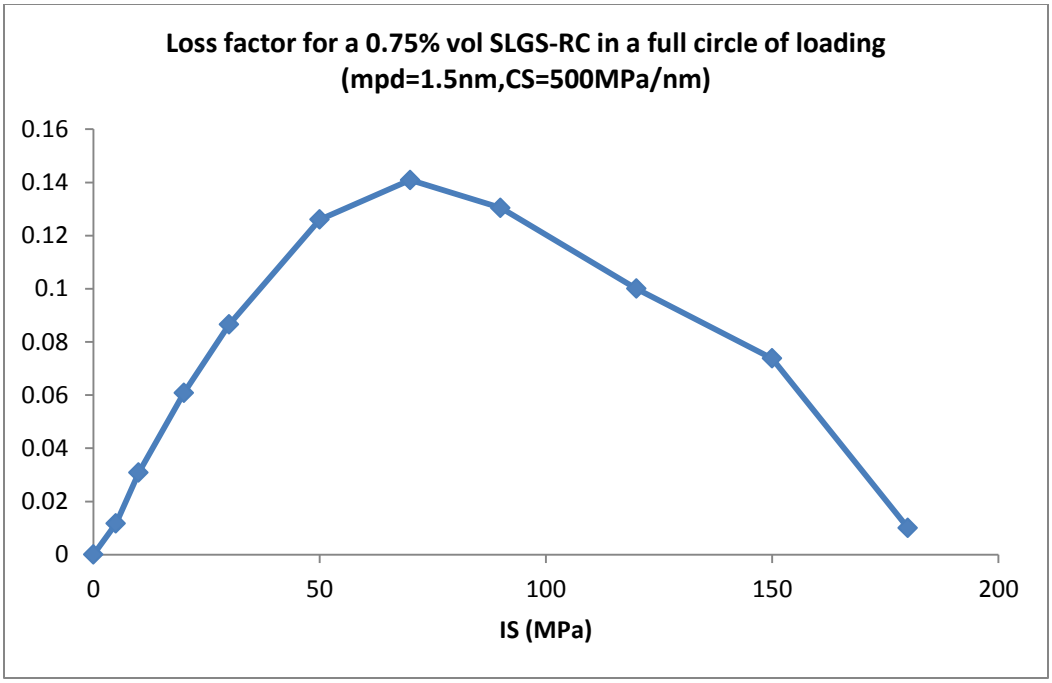

Figure 34: Loss factor of the SLGS-RC in cyclic loading conditions with respect to different IS values

Therefore, damping properties along with the stiffness of the SLGS-RC are found to be highly affected by the IS values. A similar dependence of the loss factor on the IS values is presented in CNT-RC studies [21,27].

4.4 The Effect of the Wrinkles

Randomly wrinkled SLGS with different maximum amplitudes have been considered. All of the wrinkled SLGS have been generated with the same frequency parameters on a 100x100nmSLGS. Along a straight line on a SLGS a random wave is generated as:

$$f(x) = A(\cos(10x + p1) + \sin(10x + p2) + \cos(20x + p3) + \sin(20x + p4))$$

Where A is a constant that can be altered to simulate high and low amplitude waves and p is a random initial phase between 0 and 2π. The maximum wave amplitudes (mwa) with respect to the A constant for one run of the mesh generator, are calculated as:

A	0	1	5	10	15	20	30	40	50	55
Mwa (nm)	0	0.3	1.4	2.5	4.2	5.7	8.1	14	16.7	18.9

Randomly generated waves for different values of A are depicted in Figure 35. The scale difference in the axis of vertical deflection is noted as A increases.

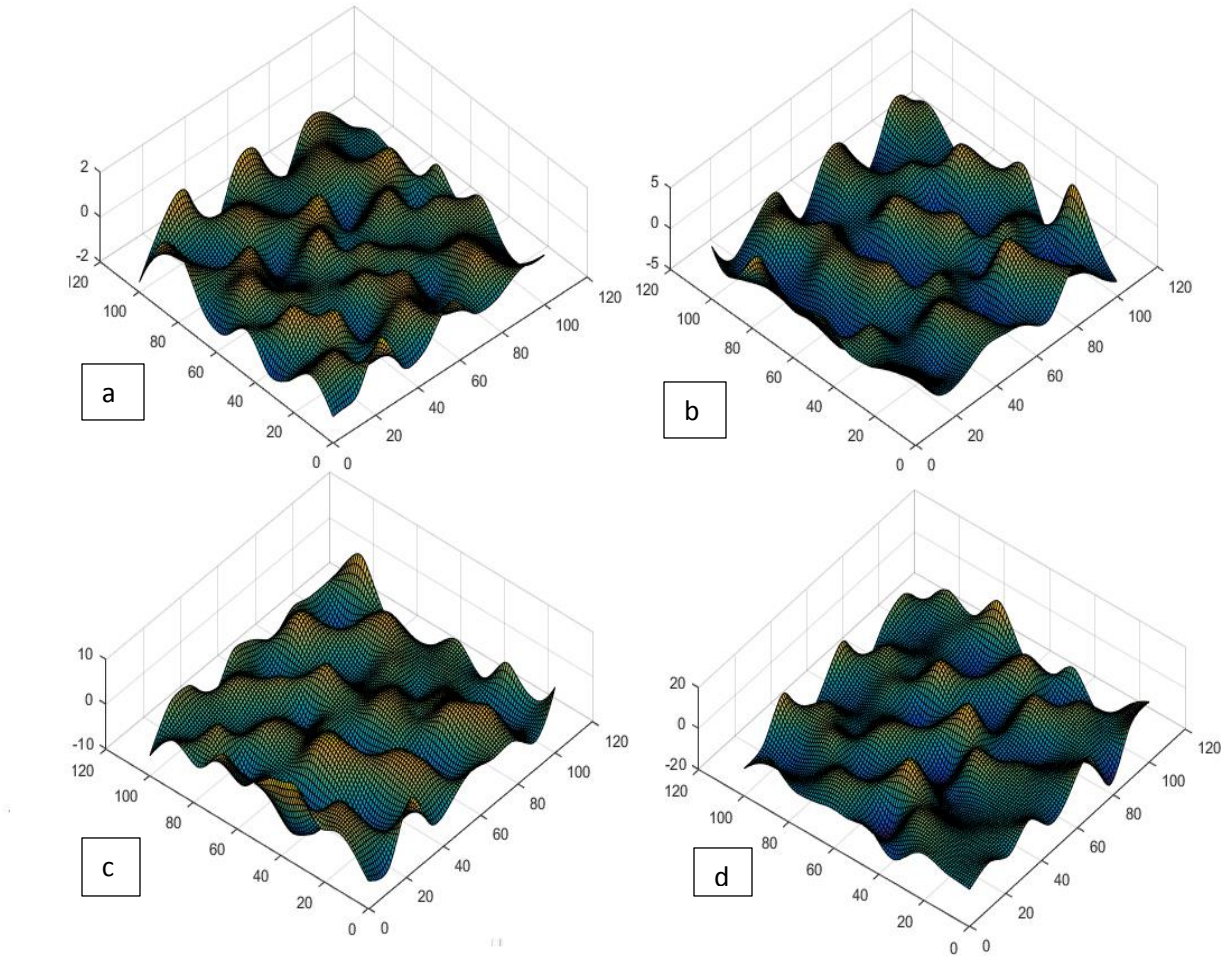

Figure 35: Randomly generated wavy SLGS for different A amplitude parameters a) A=5, b)A=15, c)A=30 and d)A=55.

The stress-strain response for the wavy SLGS-RC and the Young's modulus enhancement are depicted in Figures 36 and 37 respectively. Slight waviness lead to negligible changes compared to straight waves, however as the amplitude magnification constant A increases, reduction in stiffness is observed. A similar mechanical behavior has been observed in wavy CNT-RCs [21,27]. It is noted that no damage has been simulated in the present paragraph, with embedded element techniques used to model the nanocomposite.

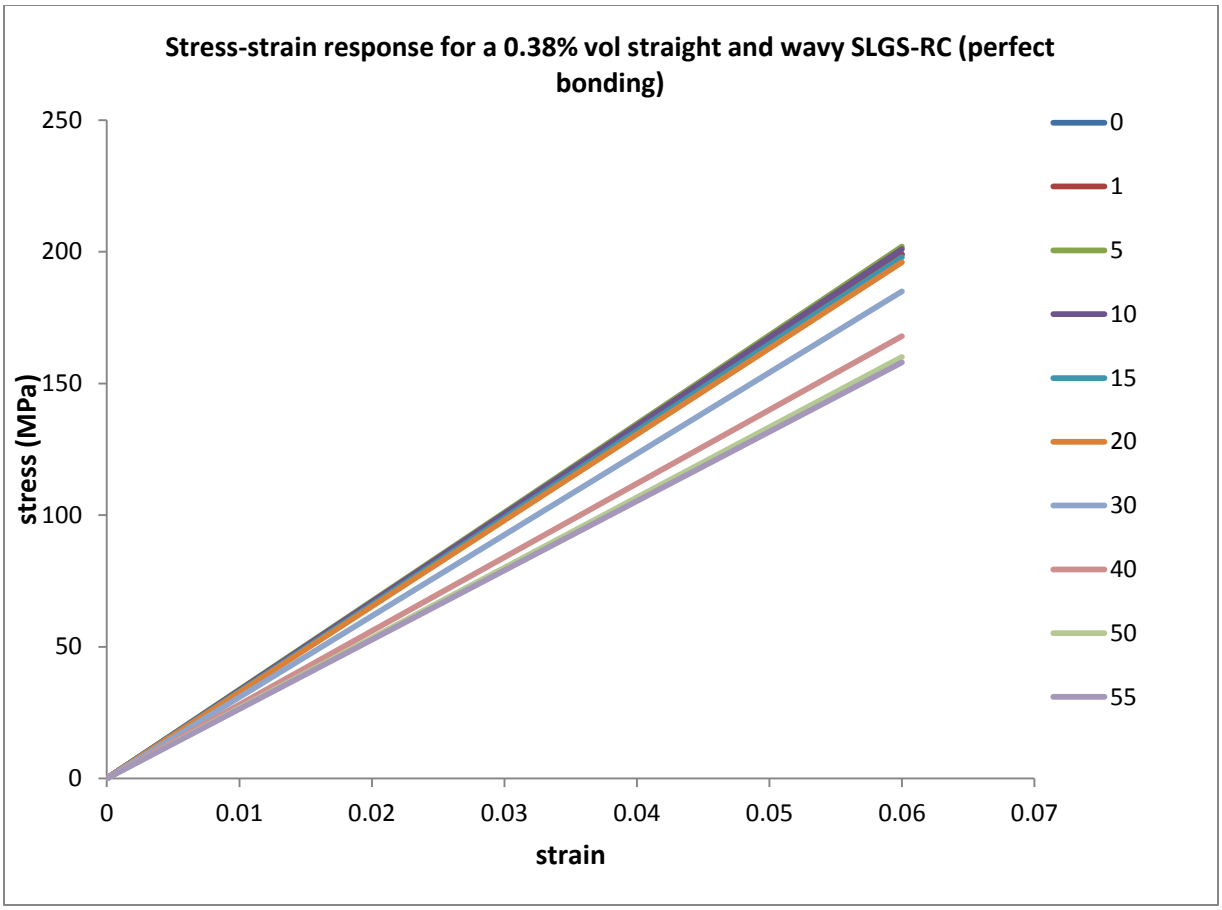

Figure 36: The effect of wrinkles on a stress-strain response of the SLGS-RC

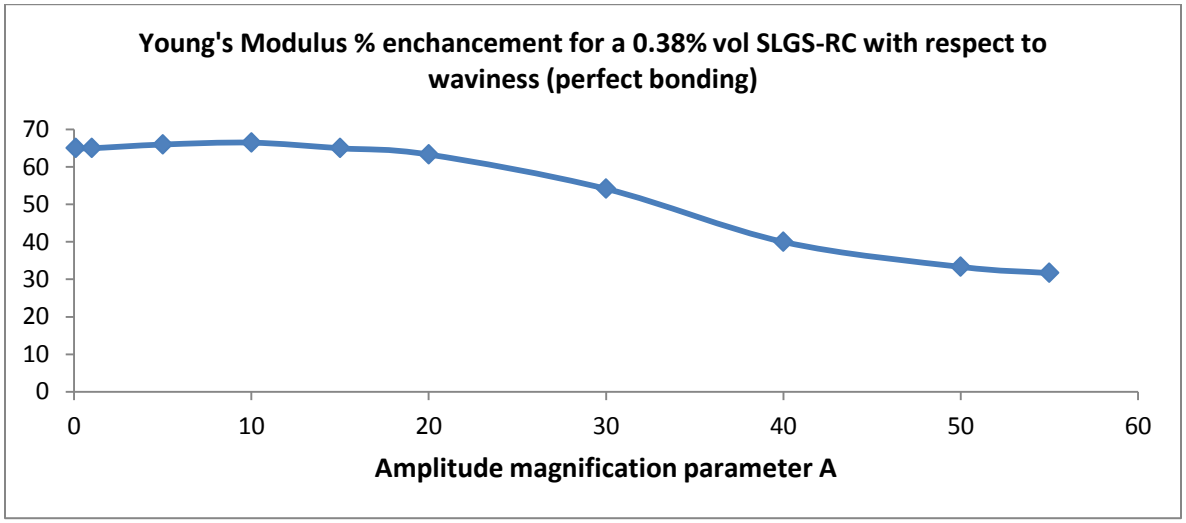

Figure 37: Young's modulus enhancement of the nanocomposite for different random wave amplitude parameters

The reduction in stiffness, could be attributed to the smaller effective membrane area due to the sheet orientation. Figure 38 shows the stress distribution on a wrinkled and on a straight SLGS of the RC. As the plate behavior has small stiffness compared to the membrane, wavy areas have a lower contribution to the RC stiffness.

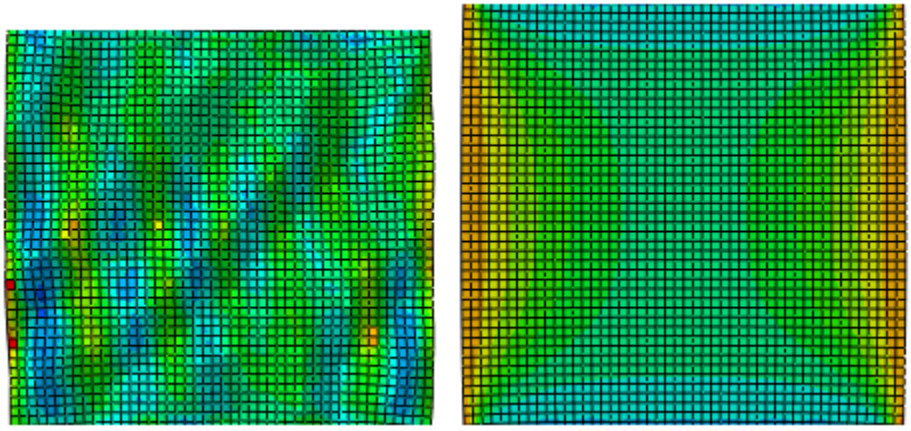

Figure 38: Tensile stress distributions on a SLGS, a) wrinkled, b) straight. Bright areas indicate high stress, while dark areas indicate low stress

5. Conclusions

In the present work, a multiscale finite element model has been developed for the study of the mechanical behavior of graphene nanocomposites. Equivalent continuum mechanics methods were applied for modeling interatomic interactions, providing a linkage between the small atomic scales and larger sizes with computational efficiency. The interactions between carbon atoms in a SLGS lead to a continuum shell behavior, which can be represented with the ESE. The interactions between the matrix and graphene, which define the ILTM, are modeled with a continuum cohesive zone. The cohesive zone can be used as general method of simulation for all kinds of matrix-filler bonding, weak or strong. The finite element model of the ESE embedded in a polymer matrix is validated by observing its mechanical behavior with other ILTM models both GS-RC and CNT-RC. Cohesive damage leads to a non-linear stress-strain response due to failed bonds. Debonding phenomena in the SLGS-RC result in the same behavior as delamination in conventional composites. The values of the cohesive strength have a direct impact on the mechanical behavior, with stronger bonds leading to better enhancement of the nanocomposite, and bonds that can be regenerated leading to hysteresis loops in cyclic loadings. Damping occurring from hysteresis, has been found depend on the interfacial strength and maximized in a limited range of strength values. Wrinkles on graphene lead to reduced stiffness of the nanocomposite, which depends on the waviness of the sheets. The ESE approach with a cohesive zone between matrix and filler can capture all of these phenomena with a low computational cost. As future work could be proposed the derivation of the cohesive damage initiation and propagation parameters, for specific bond types from molecular dynamics or experimental data designed for this purpose.

6 References

[1] Anchal Srivastava, Charudatta Galande, Lijie Ci, Li Song, Chaitra Rai, Deep Jariwala, Kevin F. Kelly, and Pulickel M. Ajayan, Novel Liquid Precursor-Based Facile Synthesis of Large-Area Continuous, Single, and Few-Layer Graphene Films, Chemistry of Materials, May 2010

[2] Albert Dato, Velimir Radmilovic, Zonghoon Lee, Jonathan Phillips, and Michael Frenklach, Substrate-Free Gas-Phase Synthesis of Graphene Sheets, Nano Letters, 2008, Vol.8, No7

[3] Alfonso Reina, Xiaoting Jia, John Ho, Daniel Nezich, Hyungbin Son, Vladimir Bulovic, Mildred S. Dresselhaus, and Jing Kong, Large Area, Few-Layer Graphene Films on Arbitrary Substrates by Chemical Vapor Deposition, *Nano Letters.*, 2009, 9 (1), 30-35

[4] I.A.Ovid'ko, MECHANICAL PROPERTIES OF GRAPHENE, Rev.Adv. Mater. Sci. 34 (2013) 1-11

[5] Changgu Lee, Xiaoding Wei, Jeffrey W. Kysar, James Hone, Measurement of the Elastic Properties and Intrinsic Strength of Monolayer Graphene, *Science* 321, 385 (2008);

[6] Mohammad A. Rafiee, Javad Rafiee, Zhou Wang, Huaihe Song, Zhong-Zhen Yu, and Nikhil Koratkar, Enhanced Mechanical Properties of Nanocomposites at Low Graphene Content, ACS NANO 2009, Vol.3, No12

[7] Kin-Tak Lau, David Hui, The revolutionary creation of new advanced materials –carbon nanotubes composites, Composites Part B 33 (2002) 263-277

[8] Jaewon Hwang , Taeshik Yoon , Sung Hwan Jin , Jinsup Lee , Taek-Soo Kim ,Soon Hyung Hong and Seokwoo Jeon, Adv. Mater. 2013, 25, 6724–6729

[9] Stephen F. Bartoluccia, Joseph Parasa, Mohammad A. Rafieeb, Javad Rafieec, Sabrina Leea, Deepak Kapoora, Nikhil Koratkarc, Graphene–aluminum nanocomposites, Materials Science and Engineering A 528 (2011) 7933– 7937

[10] Jonathan N. Coleman, Umar Khan, Werner J. Blau, Yurii K. Gun'ko, Small but strong: A review of the mechanical properties of carbon nanotube–polymer composites, Carbon 44 (2006) 1624–1652

[11] F. Wang, Y. Zhang, B.B. Zhang, R.Y. Hong, M.R. Kumar, C.R. Xie, Enhanced electrical conductivity and mechanical properties of ABS/EPDM composites filled with graphene, Composites Part B 83 (2015) 66e74

[12] Guoxin Cao, Atomistic Studies of Mechanical Properties of Graphene, *Polymers* 2014, *6*, 2404-2432

[13] Gregory Van Lier, Christian Van Alsenoy, Vic Van Doren, Paul Geerlings, Ab initio study of the elastic properties of single-walled carbon nanotubes and graphene, Chemical Physics Letters 326 _2000. 181–185

[14] P. Zhao and G. Shi, Study of Poisson's Ratios of Graphene and Single-Walled Carbon Nanotubes Based on an Improved Molecular Structural Mechanics Model, SL, vol.5, no.1, pp.49-58, 2011

[15] Mahmood M. Shokrieh, Roham Rafiee, Prediction of Young's modulus of graphene sheets and carbon nanotubes using nanoscale continuum mechanics approach, Materials and Design 31 (2010) 790–795

[16] K.I.Tserpes, P.Papanikos, Finite element modeling of single-walled carbon nanotubes, Composites: Part B 36 (2005) 468–477

[17] Chunyu Li, Tsu-Wei Chou, A structural mechanics approach for the analysis of carbon nanotubes, International Journal of Solids and Structures 40 (2003) 2487–2499

[18] Michele Meo, Marco Rossi, Prediction of Young's modulus of single wall carbon nanotubes by molecular-mechanics based finite element modeling, Composites Science and Technology 66 (2006) 1597–1605

[19] Xiaoxing Lu, Zhong Hu, Mechanical property evaluation of single-walled carbon nanotubes by finite element modeling, Composites: Part B 43 (2012) 1902–1913

[20] Hsien-Chie Cheng, Yang-Lun Liu, Chun-Hung Wu, Wen-Hwa Chen, On radial breathing vibration of carbon nanotubes, Comput. Methods Appl. Mech. Eng. 199 (2010) 2820–2827

[21] D.N. Savvas , V. Papadopoulos, M. Papadrakakis, The effect of interfacial shear strength on damping behavior of carbon nanotube reinforced composites, International Journal of Solids and Structures 49 (2012) 3823–3837

[22] P. Papanikos, D.D. Nikolopoulos, K.I. Tserpes b, Equivalent beams for carbon nanotubes, Computational Materials Science 43 (2008) 345–352

[23] Wlasnosci Srezyste Kompozytow Wzamacnianych Krzywoliniowymi Nanonurkami Weglowymi, Elastic properties of composites reirforced by wavy carbon nanotubes, Machanics and Control Vol.30 No.4 2011

[24] Gaoming Dai, Leon Mishnaevsky Jr, Graphene reinforced nanocomposites: 3D simulation of damage and fracture, Computational Materials Science 95 (2014) 684–692

[25] Huang, X., Qi, X., Boey, F. Y. C., & Zhang, H. (2012) Graphene-Based Composites. Chemical Society Reviews, 41, 666-686.

[26] Bin Shen, Wentao Zhai, Mimi Tao, Dingding Lu, Wenge Zheng, Chemical functionalization of graphene oxide toward the tailoring of the interface in polymer composites, Composites Science and Technology 77 (2013) 87–94

[27] Dimitris Savvas, Vissarion Papadopoulos, NONLINEAR MULTISCALE HOMOGENIZATION OF CARBON NANOTUBE REINFORCED COMPOSITES WITH INTERFACIAL SLIPPAGE, Journal for Multiscale Computational Engineering, 12 (4): 271–289 (2014)

[28] Analysis of skin-stiffener debonding under tension, Abaqus Example Problems Manual, 1.4.5, version 6.7

[29] Delamination analysis of laminated composites, Abaqus Benchmarks Manual, 2.7.1, version 6.12

[30] Mandar Kulkarni, David Carnahan, Kapil Kulkarni, Dong Qian, Jandro L. Abot, Elastic response of a carbon nanotube fiber reinforced polymeric composite: A numerical and experimental study, Composites: Part B 41 (2010) 414–421

[31] Maziar Ramezani, Juan Vilches and Thomas Neitzert, Pull-out behavior of galvanized steel strip in foam Concrete, International Journal of Advanced Structural Engineering 2013, 5:24

[32] Machida K, Principles of Molecular Mechanics, Tokyo: Kodansha and John Wiley & Sons Co-publication, 1999.

[33] Cornell W.D., Cieplak P., Bayly C.I., A second generation force-field for the simulation of proteins, nucleic-acids, and organic-molecules, Journal of American Chemical Society, Vol. 117, pp. 5179–5197, 1997

[34] Wen-Hwa Chen, Hsien-Chie Cheng, Yang-Lun Liu, Radial mechanical properties of single-walled carbon nanotubes using modified molecular structure mechanics, Computational Materials Science 47 (2010) 985–993

[35] Cengiz Baykasoglu, Ata Mugan, Dynamic analysis of single-layer graphene sheets, Computational Materials Science 55 (2012) 228–236

[36] Ricardo Faccio, Luciana Fernández-Werner, Helena Pardo, Cecilia Goyenola, Pablo A. Denis and Álvaro W. Mombrú (2011). Mechanical and Electronic Properties of Graphene Nanostructures, Physics and Applications of Graphene - Theory, Dr. Sergey Mikhailov (Ed.), ISBN: 978-953-307-152-7

[37] Ali Hemmasizadeh, Mojtaba Mahzoon, Ehsan Hadi, Rasoul Khandan, A method for developing the equivalent continuum model of a single layer graphene sheet, Thin Solid Films 516 (2008) 7636–7640

[38] Gregory M. Odegard, Thomas S. Gates, Lee M. Nicholson, Kristopher E. Wise, Equivalent-continuum modeling of nano-structured materials, Composites Science and Technology 62 (2002) 1869–1880

[39] Μ.Παπαδρακάκης, Ανάλυση Φορέων με τη Μέθοδο των Πεπερασμένων Στοιχείων, Αθήνα 1996

[40] Young W. Kwon, Hyochoong Bang, The Finite Element Method Using MATLAB, CRC Press 1997, ISBN:0-8493-9653-0

[41] Y. Chandra, F. Scarpa, R. Chowdhury, S. Adhikari, J. Sienz, Multiscale hybrid atomistic-FE approach for the nonlinear tensile behaviour of graphene nanocomposites, Composites: Part A 46 (2013) 147–153

[42] Yogeeswaran Ganesan, Cheng Peng, Yang Lu, Phillip E. Loya, Padraig Moloney, Enrique Barrera, Boris I. Yakobson, James M. Tour, Roberto Ballarini and Jun Lou, Interface Toughness of Carbon Nanotube Reinforced Epoxy Composites, ACS Appl. Mater. Interfaces 2011, 3, 129–134

[43] K.I.Tserpes, P.Papanikos, G.Labeas, G.Pantelakis, Multi-scale modeling of tensile behavior of carbon nanotube-reinforced composites, Theoretical and Applied Fracture Mechanics 49 (2008) 51–60

[44] Mahmood M. Shokrieh, Roham Rafiee, On the tensile behavior of an embedded carbon nanotube in polymer matrix with non-bonded interphase region, Composite Structures 92 (2010) 647–652

[45] M. Safaei, A. Sheidaei, M. Baniassadi, S. Ahzi , M. Mosavi Mashhadi, F. Pourboghrat, An interfacial debonding-induced damage model for graphite nanoplatelet polymer composites, COMPUTATIONAL MATERIALS SCIENCE, JANUARY 2015

[46] L.Y.Jiang, Y.Huang, H.Jiang, G.Ravichandran, H.Gao, K.C Hwang, B. Liu, A cohesive law for carbon nanotube/polymer interfaces based on the van der Waals force, Journal of the Mechanics and Physics of Solids 54 (2006) 2436–2452

[47] Yancheng Zhang, Xiaoying Zhuang, Jacob Muthu, Tarek Mabrouki, Michaël Fontaine, Yadong Gong, Timon Rabczuk, Load transfer of graphene/carbon nanotube/polyethylene hybrid nanocomposite by molecular dynamics simulation, Composites: Part B 63 (2014) 27–33

[48] Feng Liu, Ning Hu, Huiming Ning, Yaolu Liu, Yuan Li, Liangke Wu, Molecular dynamics simulation on interfacial mechanical properties of polymer nanocomposites with wrinkled graphene, Computational Materials Science 108 (2015) 160–167

[49] A.P.Awasthi, D.C.Lagoudas, D.C.Hammerand, Modelling and Simulation in Materials Science and Engineering, Published 18 November 2008, 2009 IOP Publishing Ltd, Modelling and Simulation in Materials Science and Engineering, Volume 17, Number 1

[50] AN ATOMISTIC STUDY OF THE MECHANICAL BEHAVIOR OF CARBON NANOTUBES AND NANOCOMPOSITE INTERFACES A Dissertation by AMNAYA P. AWASTHI Submitted to the Office of Graduate Studies of Texas A&M University in partial fulfillment of the requirements for the degree of DOCTOR OF PHILOSOPHY December 2009

[51] R.Hill, Elastic Properties of Reinforced Solids: Some Theoretical Principles, J.Mech.Phys.Solids, 1963 Vol.11, p.p.357-372, Pergamon Press L.t.d.

[52] Y.J. Liu , X.L. Chen, Evaluations of the effective material properties of carbon nanotube-based composites using a nanoscale representative volume element, Mechanics of Materials 35 (2003) 69–81

[53] Modeling with cohesive elements, Abaqus Analysis User's Manual, 26.5.3, version 6.7

[54] Davila, C. G., and P. P. Camanho, “Analysis of the Effects of Residual Strains and Defects on Skin/Stiffener Debonding using Decohesion Elements,” SDM Conference, Norfolk, VA, April 7–10, 2003.

[55] Krueger, R., M. K. Cvitkovich, T. K. O'Brien, and P. J. Minguet, “Testing and Analysis of Composite Skin/Stringer Debonding under Multi-Axial Loading,”Journal of Composite Materials, vol. 34, no.15, pp. 1263–1300, 2000

[56] Defining the constitutive response of cohesive elements using a traction-separation description, Abaqus Analysis User's Manual, 26.5.6 , version 6.7